AD-A190 870 EXPERIMENTAL INVESTIGATION OF THE HYPERSONIC FLOW OVER A SIX FINNED CONFI..(U) NEW YORK UNIV WESTBURY ANTONIO FERRI LABS A M AGNONE ET AL. JUN 87 ARO-20723.3-EG 1/1

UNCLASSIFIED DAAG29-83-K-0115 F/G 16/2.1 NL

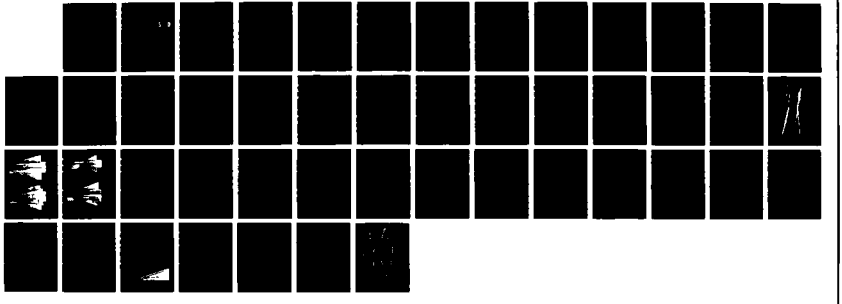

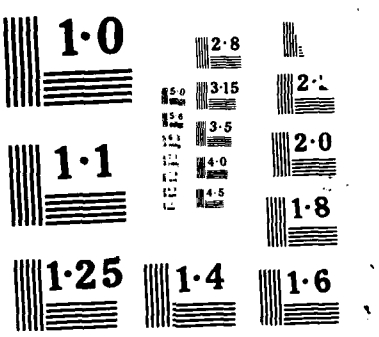
1·0
1·1
1·25
2·8
3·15
3·5
4·0
4·5
2·0
1·8
1·4
1·6

EXPERIMENTAL INVESTIGATION OF THE HYPERSONIC FLOW OVER A SIX FINNED CONFIGURATION

FINAL REPORT

A.M. Agnone, V. Zakkay, and K.S. Parmar

JUNE 1987

U.S. ARMY RESEARCH OFFICE

DASG29-83-K-0115

NEW YORK UNIVERSITY
Antonio Ferri Laboratories
Westbury, L.I.N.Y. 11590

UNCLASSIFIED

SECURITY CLASSIFICATION OF THIS PAGE (When Data Entered)

REPORT DOCUMENTATION PAGE		READ INSTRUCTIONS BEFORE COMPLETING FORM
1. REPORT NUMBER ARO 20723.3-EG	2. GOVT ACCESSION NO. NA	3. RECIPIENT'S CATALOG NUMBER NA
4. TITLE (and Subtitle) Experimental Investigation of the Hypersonic Flow Over a Six Finned Configuration		5. TYPE OF REPORT & PERIOD COVERED 6. PERFORMING ORG. REPORT NUMBER
7. AUTHOR(s) A.M. Agnone, V. Zakkay, and K.S. Parmar		8. CONTRACT OR GRANT NUMBER(s) DAAG29-83-K-0115
9. PERFORMING ORGANIZATION NAME AND ADDRESS New York University Antonio Ferri Laboratories 425 Merrick Avenue-Westbury, L.I.N.Y. 11590		10. PROGRAM ELEMENT, PROJECT, TASK AREA & WORK UNIT NUMBERS NA
11. CONTROLLING OFFICE NAME AND ADDRESS U. S. Army Research Office P. O. Box 12211 Research Triangle Park, NC 27709-2211		12. REPORT DATE October 1986 13. NUMBER OF PAGES
14. MONITORING AGENCY NAME & ADDRESS(if different from Controlling Office)		15. SECURITY CLASS. (of this report) UNCLASSIFIED 15a. DECLASSIFICATION/DOWNGRADING SCHEDULE

16. DISTRIBUTION STATEMENT (of this Report)

Approved for public release; distribution unlimited.

17. DISTRIBUTION STATEMENT (of the abstract entered in Block 20, if different from Report)

NA

18. SUPPLEMENTARY NOTES

The view, opinions and/or findings contained in this report are those of the author(s) and should not be construed as an official Department of the Army position, policy, or decision, unless so designated by other documentation.

19. KEY WORDS (Continue on reverse side if necessary and identify by block number)

Hypersonic, Aerodynamics, Fluid Mechanics, Navier Stokes, Code Validation, Finned Configuration, Experiment

20. ABSTRACT (Continue on reverse side if necessary and identify by block number)

DD FORM 1 JAN 73 1473 EDITION OF 1 NOV 65 IS OBSOLETE

UNCLASSIFIED

SECURITY CLASSIFICATION OF THIS PAGE (When Data Entered)

ABSTRACT

Experimental data of the flow field over a six-finned configuration are compared with computations from an inviscid Euler code and a parabolized Navier-Stokes (PNS) code to assess their accuracy. The experiments were conducted with a smooth and a grooved cylinder in a hypersonic (M=6.5) wind tunnel. Surface oil flow patterns, surface pressures, local heat flux rates and flow field pitot surveys are presented. The PNS computations are in good agreement with the measurements in the inviscid regions. However, significant differences are noted in the viscous regions possibly due to nose tip bluntness effects and the associated entropy layer.

TABLE OF CONTENTS

FOREWORD

This report, prepared by New York University Antonio Ferri Laboratories, under U.S. Army Research Contract No. DAAG29-83-K-0115, presents the research and data analysis from wind tunnel tests conducted on a six finned configuration. The test program was conducted in the Antonio Ferri M = 6.0 Hypersonic Facility at Westbury, L.I.N.Y.

The Scientific Program Officer was Dr. Robert E. Singleton, and the Technical Liason was Dr. Walter Sturek of the U.S. Army Ballistics Research Laboratories, Aberdeen, Maryland. The parabolized Navier Stokes Code Computations presented herein were performed by Dr. Paul Weinacht.

The authors wish to acknowledge the contributions of Mr. Harold Clisset. This report covers the work performed from October 1, 1983 to May 31, 1987.

LIST OF SYMBOLS

A	Area
A_{cyl}	Cross sectional area of cylinder = $1/4\ \pi\ D^2_{cyl}$
A_f	Planform area of a single fin
b	Semi-span of a fin = 8.379 cm (3.299 in)
C_z	Axial force coefficient = $F_z / q_\infty A_{cyl}$
C_l	Rolling moment coefficient = $l / q_\infty A_{cyl} D_{cyl}$
C_N	Normal force coefficient = $N/q_\infty A_{cyl}$
C_m	Pitching moment coefficient = $m/q_\infty\ A_{cyl}\ D_{cyl}$
D_{cyl}	Cylinder diameter = 10.16 cm (4.00 inches)
F_Z	Axial force due to aerodynamic load
L	Model length = 112.93 cm = 44.46 inches
m	Pitching moment
M	Mach number
N	Normal force due to aerodynamic load
P	Static (surface) pressure
P_o	Freestream stagnation pressure
P_{T2}	Local pitot pressure
q_∞	Freestream dynamic pressure = $1/2\ \rho_\infty V^2_\infty$
$\dot{q}_w$	Heat transfer rate = kW/m^2 = (0.0881 Btu/ft^2 sec)
r, R	Radius or radial distance from model axis
R_e	Unit Reynolds number = $\rho_\infty V_\infty / \mu_\infty$

R_{LE}	Fin leading edge radius (see Fig. 1)
R_n	Nose cone-tip radius = 0.451 cm (0.1818 inches)
T	Temperature
T_o	Freestream stagnation temperature
T_w	Model wall (surface) temperature
V_∞	Freestream velocity
x,y,z	Body fixed Cartesian coordinate system
x,r,φ	Body fixed cylindrical coordinate system
Z	Axial component of aerodynamic force

GREEK SYMBOLS

α	Angle of attack
γ	Ratio of specific heats for air
Λ	Fin leading edge sweep back angle = 72.7^o
φ	Meridional angle from the most windward ray
ϕ	Model roll angle
ρ	Mass density
μ	fluid (air) viscosity

SUBSCRIPTS

∞	Freestream conditions
cyl	cylinder
w	model wall conditions

I - INTRODUCTION

Reliable computations of the aerodynamic coefficients of hypersonic missiles require the use of analytical tools, such as the three dimensional parabolized Navier-Stokes (PNS) code being developed by Weinacht, 1985. In this code, the steady thin layer approximations to the N-S equations written in strong conservation form in generalized coordinates (using a wrap around grid), are solved using an approximately factored, implicit, finite difference numerical algorithm. An initial data plane, generated from a conical flow, is used to march the solution downstream. A fully turbulent boundary layer, based on a modified two-layer algebraic turbulence model, is used. Weinacht has applied the code to compute aerodynamic coefficients of i) a Secant-Ogive-Cylinder-Boattail configuration at 6.3 deg. angle of attack, at Mach 3.0, with and without spin, ii) a long slender finned body configuration at Mach numbers 3, 4 and 5 and for 2 deg. angle of attack. Good agreement with range data and predictions from an inviscid code was found.

The objective of this investigation is to provide detailed experimental data about the flow over a six-finned configuration for comparison with computations using this code. The comptutations for the present configuration were performed only for zero angle of attack on a Cray XMP super-computer with improved grid resolution of the viscous layer on the fins and without using large smoothing. To interpret the angle of attack data, an Euler code (SWINT) Wardlaw, 1983, was used. The SWINT code treats configurations with forward and aft fins as thin surfaces located in meridional planes. A finite difference marching technique is used. Supersonic flow is assumed throughout the flow field. The cross-flow separation on the leeward surfaces of the body is modeled semi-empirically.

II - EXPERIMENTAL APPARATUS AND TEST CONDITIONS

The experiments were conducted with a 10.16 cm diameter model, Fig. 1. It had an 8 deg slightly blunted half angle cone, followed by a long cylinder, and six blunted and swept fins. Tests were conducted with a smooth cylinder and one with sub-caliber roughness (sabot grooves) see detail in Fig. 1. A typical fin cross-section, SECTION A-A Fig. 1, shows that the 60% blunt fin leading edge is followed by a 7 deg symmetrical wedge and a planar section. An aft 7^o expansion surface, near the trailing edge on only one side of the fin, provides an unbalanced pressure which induces a rolling moment. The trailing edges are rounded similar to the leading edge. A thick (~1cm) boundary layer in the fins region develops at wind tunnel conditions.

The experiments were performed in the Mach 6.5 blowdown facility, which was operated at nominally 5.5 MPa (800 psia) stagnation pressure, and with 500 K stagnation temperature air. The corresponding free stream unit Reynolds number based on the model diameter was $Re_D = 3.3 \times 10^6$. The model wall was at ambient temperature; hence $T_w/T_o = 0.60$. Tests were conducted for model incidence angles, $\alpha = 0^o$, 5^o and 10^o, and fin roll angles, $\phi = 0^o$ (two fins in the pitch plane) and 30^o (two fins in the horizontal plane).

The wind tunnel model was instrumented with 150 surface pressure taps on two facing fin surfaces, and the included cylindrical surface. A total of 74 thin-skin heat transfer gauges were installed on two facing fin surfaces diametrically opposite to the pressure instrumented fins. In the last test series, two HY-CAL Engineering heat flux gauges were installed diametrically opposite to one another on the cylinder one caliber upstream of the fins to accurately measure the reference heat flux on the cylinder.

III - DATA PRESENTATION AND COMPARISON WITH ANALYSIS

Three series of tests have been conducted with the smooth cylinder model: 1) oil flow tests to obtain surface flow patterns; 2) surface pressures and heat flux distributions on all fins surfaces; and 3) flow field surveys around a typical fin. A fourth test series was conducted with the grooved model to asses the effects of the grooves. In this last test series, only items 2 and 3 above were measured for a zero angle of attack only. Shadowgraph photographs of flow regions rear the fins were also taken.

A - Surface Flow Patterns

The streamline patterns on the various fins surfaces, Fig. 2, computed with the PNS code for zero angle of attack, show the effects of the fins leading edge bluntness and sweepback. A corner flow region at the juncture of the fin with the cylindrical body is also evident. The observed flow patterns were similar to these. Unfortunately, the photograph was not as clear. Hence it is not presented here. On the cone and cylinder, the streamlines are aligned with the generatrices.

Typical oil flow patterns for $\alpha \approx 5^{o}$ are presented in Figs. 3a and 3b for $\phi = 0^{o}$ and 30^{o} respectively. The patterns show adjacent fin shock traces on the cylinder intersecting at about one third of the fins root chord. On the leeward fin surfaces, there are three flow regions: the first is associated with the blunt fins leading edges which are supersonic (M_N = 2.); the second region is the "delta" flow region, and the third is associated with the corner region formed by the juncture of the fin and body. The distinct line separating the leading edge region and the delta flow region may be due to the formation of a swept recompression shock and a vortical structure in

the boundary layer beneath this shock. Similar structures have been computed by Rizzi, 1985, for a delta wing using a PNS code. The surface streamlines near the fin's leading edges are similar to the flow over a swept infinite cylinder. The corner region on the leeward surfaces occupies a considerable (25-30%) portion of the fin's surface, and shows vortical structures. These regions possess conical properties up to where the adjacent fin shocks interact.

Typical oil flow patterns obtained for $\alpha = 10^{o}$ and for $\phi = 0^{o}$ and 30^{o} roll orientations are shown in Figs. 4a and 4b respectively. At this attitude, the flow over the cone and cylinder is separated on the leeward surfaces from about $\varphi = 100^{o}$ and starting almost from the nose tip. For $=0^{o}$, the surface patterns (Fig. 4a) show the body separation region interaction with the fin located at $\varphi = 120^{o}$. The body separation line wets the leeward surface of the fin located at $\varphi = 60^{o}$ from the most windward ray.

At a 30^{o} roll angle, the body separation line remains above the horizontal fin. The top view, Fig. 4b, shows the secondary separation zone is contained between the $\varphi = 150^{o}$ and $\varphi = 210^{o}$ fins. The leeside surface patterns on the horizontal fins show the leading edge region is rather narrow; while the corner flow region spreads at about a 4.5^{o} angle. The major portion of the surface is occupied by the "delta" flow region. The limiting streamlines average slope is about 33^{o}.

B 1 -Surface Pressure Data - Zero Angle of Attack

The measured pressure distribution from several tests for zero angle of attack, along a ray on the cylinder midway between adjacent fins ($\varphi = 30^{o}$) is compared in Fig. 5 with the PNS and SWINT computations. The measured

pressures with both the smooth and rough cylinder are shown. In the SWINT calculation, sharp fins were used. Hence the maximum pressure rise is not as observed and is shifted downstream. In the PNS computation, the boundary layer was assumed to be turbulent from the cone tip. The pressure distribution shows a peak pressure, due to the fin's bow shock, which is slightly greater than the measurements. Similar differences between the measured and computed values of surface pressures have been observed by Rizzi, 1985, in conjunction with the flow over the upper surface of a delta wing. The pressure suction peak which is produced by the formation of a leading edge vortex and the subsequent development into a recompression shock was found to increase as the computational mesh diminished (Figs. 6 and 7, Rizzi). Whereas the observed pressure suction peak is decreased substantially since "..the experiment contained a secondary vortex (produced by the presence of the boundary layer) which is known to truncate the peak and shift it inboard," Rizzi, p. 152. Similar compression rarefaction phenomena associated with the wetting of the boundary layer on the cylinder by the fins bow shocks may have caused the differences noted in Fig. 5. Also, upstream influence in the boundary layer, flow asymmetry due to small yaw/angle of attack, tunnel flow non-uniformity and data accuracy may have contributed to the differences.

The measured pressures on a fin surface are compared with the PNS and SWINT computations in Fig. 6 for several spanwise sections on the fin. The pressure on the 7^{o} wedge (SECTION B-B) is accurately reproduced by both codes. Further outboard, the wedge pressure appears to be "washed-out" by an expansion. The pressure on the fin leading edge stagnation line computed with the PNS code is compared with the measured values in Fig. 7. Near the

edge of the boundary layer (SECTION C-C), the measured leading edge pressure from several tests varied from 4.5 to 6.0 p_∞. This discrepancy may be due to the differences in the boundary layer structure used in the PNS code (fully turbulent) and the actual boundary layer on the model (see flow profiles). Outside of the viscous layer and downstream of the leading edge regions, the pressures computed on the fins surfaces agree with the measured values within the measurement error. On the expansion surface near the trailing edge, the SWINT code (SECTIONS B-B and D-D) is shown to indicate the pressure level there. The measured pressure along the fin trailing edge line varied between 0.4 and 0.6 p_∞. The SWINT code appears to predict (SECTION D-D) a secondary recompression slightly downstream of the 7^o expansion wedge. This is more evident at angle of attack and appears to coincide with the swept recompression shock near the leading edge and observed in the oil flow patterns, FIG. 3.

B 2 - Angle of Attack Data

The pressure distributions around the smooth cylinder, at an axial station (Z/D_{cyl} = 8.0) upstream of the fins, Fig. 8 for $\alpha = 5^o$ and 10^o, show a plateau starting near 90^o from the most windward-ray. This is indicative of cross-flow separation also at 5^o angles of attack. The SWINT code results, with cross-flow separation, are in good agreement on the windward surfaces; however, the agreement is not good on the leeward surfaces.

The pressure distributions along the most windward and leeward rays of the smooth cylinder, Fig. 9 for $\alpha = 5^o$ and 10^o, and for $\phi = 30^o$ are compared with the SWINT computations. The pressure on the most leeward ray attains a maximum value of 1.1 times free stream at about 20% of the root chord.

The differences between the SWINT and the measurements are due to the fins' leading edge bluntness. On the windward side, the pressure increases to about 1.8 times the free stream value due to the shocks produced by the fins. The pressure distribution along a side ray (= 90^{o}) for a zero fin roll angle, Fig. 10 for $\alpha = 5^{o}$, also does not agree with SWINT, due to the cross flow separation on the cylinder.

The pressure at midspan of the fins' leading edges, shown in Fig. 11 as a function of the fin roll angle and angle of attack, is compared with the pressure computed using the Rayleigh Pitot formula and the component of the free stream Mach number normal to the fin's leading edge. The agreement is fair. At zero angle of attack, the PNS code gives a value of $p_{L.E.}/p_{\infty} = 5.4$ outside of the boundary layer on the cylinder, see Fig. 7.

The measured pressure distributions on the windward and leeward surfaces of the horizontal fin along a chord at mid-span, Fig. 12, for $\alpha = 5^{o}$ and for $\phi = 30^{o}$, are compared with the inviscid SWINT code results. No PNS computations were made for this case. The pressure on the windward and leeward sides of a flat plate at 5^{o} angle of attack in a Mach 6.6 freestream are 2.14 and 0.42 times p_{∞} respectively. The SWINT computations and experimental data, downstream where leading edge bluntness effects are not significant, agree with these levels.

C - Flow Profiles

Flow field surveys at a station upstream of the fins, $Z/D_{cyl} = 8.2$, and in the pitch plane, $\varphi = 0^{o}$, were performed with a traversable pitot/static pressure probe for both the smooth and grooved cylinder. The measured

pitot pressure profiles for $\alpha = 0^o$ are compared with SWINT and PNS computations in Fig. 13a for both the smooth and grooved cylynders. The computed bow shock location and strength as well as the inviscid shock layer flow structure differ slightly from the measured values. The differences may be due to probe response error, and the use of a sharp nose cone tip in the PNS computations. Near the cylindrical body surface, the entropy layer produced by the nose tip bluntness and the boundary layer structure produce the observed differences. The influence of the grooves is evident in the boundary layer profile, Fig. 13b. A significant pressure defect is caused by the expansion-shocks train produced by the grooves. Outside of the boundary layer, a defect due to the nose tip bluntness is also evident in the measured profiles. This defect is not present in the PNS computations since these were performed with a sharp nose tip starting solution.

At 5^o angle of attack, the pitot pressure profile, Fig. 14, in the most leeward plane of symmetry shows a flow structure near $r/D_{cyl}=0.75$. At this incidence, the viscous layer on the leeward surfaces is separated from the surface. The pitot pressure profile computed with SWINT, enforcing flow separation, shows similar trends. Although the agreement is not good. The conical bow shock is virtually attenuated to zero strength on the leeward side.

The pitot profile, for $\alpha = 0^o$, at a station in the fins region, $Z/D_{cyl} = 10.7$, and midway adjacent fins, Fig. 15 for both the smooth and grooved cylinder, show a peak pressure where the fin's shock intersect. The entropy layer due to the nose tip bluntness, the boundary layer and the reflected fins shock

appear to have merged. The computations with the PNS code give a better agreement with the data than the SWINT code.

Pitot pressure surveys around a typical fin at a station two cylinder diameters downstream from the fin tip station (Z/D_{cyl} = 10.7) were made with a 72 point sectored pitot rake. Lines of constant normalized pitot pressures for $\alpha = 0^o$ in a typical 30^o sector about a fin are compared with the PNS computations in Fig. 16a and 16b for the smooth and grooved cylinder respectively. The trace of the fin shock and expansion fan emanating from the 7^o wedge expansion corner as well as the reflection of the fin shock on the body are evident. The approximate location of the boundary layer edge, determined from these and flow profile data, has also been shown on the figures for completeness. The pitot data indicates that the fin shock is not discrete. It apparently has been diffracted by the boundary layer on the cylindrical surface. Also the fin shock strength is attenuated rapidly away from the fin leading edge. The PNS computation shows a similar flow structure and greater detail in the boundary layer.

The lines of constant pitot pressure measured around the horizontal fin for a model incidence of 5^o and a 30^o fin roll angle are presented in Fig. 17 for the smooth cylinder. By comparison with the zero angle of attack, these show the fin shock is strengthened on the windward side and weakened on the leeward side . The eccentric nature of the flow upstream of the fins due to the angle of attack is apparent. Also, a region of very low pitot pressure is evident on the lee side of the horizontal fin. It is bounded by the fin surface and cylindrical body and by a thin shear layer which emanates from the 7^o expansion corner near the fin leading edge. At this incidence, the 72 point sectored pitot rake may have induced this separation on the lee side of

the horizontal fins. The oil flow pattern of the horizontal fins' leeward surfaces (SN #3 or SN #8), inserted in Fig. 17, does not show flow separation.

D - Heat Transfer Measurements

The heat flux distributions, Fig. 18, on the cylinder, midway between adjacent fins on the most windward ray, for the 30^{o} fin roll orientation and for 0^{o}, 5^{o}, and 10^{o} angles of attack, show a peak heat flux where the adjacent fin shocks intersect on the cylindrical body. The heat flux distributions computed with the flat plate reference enthalpy method (FPREM), using the surface entropy corresponding to that of the normal shock produced by the blunted nose cone are shown for comparisons. On the cylinder, the PNS code yields a value of the turbulent heat flux of 6.8 kW/m^2 (0.6 BTU/ft^2 sec). This is in good agreement with the values measured on the grooved cylinder and using the HY-CAL gauges. Whereas, this value is about twice the measured values with the smooth cylinder. This shows that the grooves effectively induced transition.

Since the heat flux depends on the test conditions, i.e. Mach number, stagnation pressure and temperature, angle of attack and model wall temperature, a sensitivity analysis was performed using the FPREM. The results may be summarized according to the following equation:

$$\bar{\dot{q}}_{w_{CYL}} = 1.0 - 5.412\,(\bar{M}-1.0) + 0.7975\,(\bar{P}_0-1.0) + 3.162\,(\bar{T}_0-1.0) -$$

$$- 2.3479(\bar{T}_w-1.0) + 3.587\,\alpha$$

In this expression, $\bar{\dot{q}}_{w_{CYL}}$ is the heat flux on the cylinder upstream of the fins normalized wrt the heat flux at the nominal test conditions: i.e. M = 6.6,

P_o=750 psia, T_o= 850°R, T_w= 530°R, and α is the angle of attack in radians. Also, the values of P_o, T_o, and T_w are normalized wrt these values in this formula. This expression gives the heat flux correction due to these parameters. That is, a 1% increase in freestream Mach number produces a 5.4% decrease in heat transfer. Similarly a 1% increase in tunnel stagnation temperature produces a 3.2% increase in heat transfer, etc... . Using this formula to account for differences in windtunnel operating conditions, the lowest value of the turbulent heat transfer that could be obtained on the cylinder upstream of the fins is about 4.0 kW/m^2. Since the heat flux measured on the smooth cylinder was about 3.1 kW/m^2, it must be concluded that fully turbulent flow was not attained on the smooth cylinder. Also, since the laminar heat transfer rate is about 1.1 kW/m^2, the flow must have been transitional. Except near the fins leading edges and the corner regions, the heat flux on the fins' surfaces was of the same order as on the cylinder.

The heat flux on the fin's leading and trailing edges at mid-span, Fig. 19, for $\alpha = 0^o$, 5^o and 10^o vary with the fins' circumferential position. The stagnation point heat transfer analysis of Reshotko and Beckwith, 1958, for the viscous flow over a swept cylinder is shown for comparison. The effects of the upstream flow due to the cylinder have been included in the analysis by correcting the fin sweepback angle by the local flow direction produced by the cone-cylinder forebody. The stagnation pressure at the fin leading edge was assumed to be that presented in Fig. 11 and calculated using the Rayleigh pitot formula with the normal component of the local Mach number. The agreement between the measured heat flux on the leading edges and that computed by this analysis appears to be good.

E - AERODYNAMIC COEFFICIENTS

The axial and normal force coefficients of the complete configuration were obtained from the measured surface pressures. The contribution due to the nose cone bluntness and the fins leading and trailing edge bluntness were estimated from empirical correlations using the approach Mach number. The axial force coefficient, C_z, variation with angle of attack is shown in Fig. 20. The 8^0 cone contribution to the axial force is about 30% of the total force; while the sharp fins thickness contribute about 18% and the fins' blunt leading edges contribute about 25%. The bluff base contributes about 15%. The remainder is due to viscous effects assuming a turbulent boundary layer everywhere. The axial force coefficient computed with the SWINT code, corrected for the bluntness and viscous effects, is shown in Fig. 20 for comparison. At zero angle of attack, the PNS code predicts an axial force coefficient of 0.12 for the pressure contribution and excluding the bluff base drag. The incremental axial force coefficient due to the viscous effects, calculated with the PNS code assuming turbulent flow everywhere and for the nominal windtunnel conditions, is 0.069.

The normal force coefficientof the complete configuration, at a 5 deg. angle of attack, yields a slope, $C_{N_{\alpha_o}}$, of about 7 per radian. The corresponding pitching moment coefficient slope is $C_{m_{\alpha_o}}$ = 4.13 per radian. The configuration develops a rolling moment due to the asymmetry of the aft portion of the fins' surfaces. The rolling moment estimated from the measured pressure data is about C_{l_0} = 0.023 at zero angle of attack.

IV - SUMMARY AND CONCLUSIONS

Surface flow patterns on a typical fin of a six-finned configuration show flow regions near the blunt leading edge, on the "delta" planform, and the corner flow region formed by the juncture of the fin and cylindrical body. On the cylinder surface, the fin shocks and expansion waves traces are evident. At 10^{o} angle of attack, cross-flow separation prevails on the leeward surfaces of the body and fins.

The measured surface pressures, and those computed using the PNS code, are in good agreement with the experimental data especially in the inviscid regions. However significant differences are noted in the viscous layer possibly due to the entropy layer produced by the nose tip bluntness and the absence of a turbulent boundary layer over the smooth cylinder model. At angle of attack, cross flow separation is evident also in the pressure measurements on the leeward surface of the cylinder. The impact pressure maps around a typical fin show various flow structures. The measured heat flux on the smooth cylinder are about half the values computed with the PNS code. This shows a transitional flow may have prevailed in this case. However, the heat flux measured on the grooved cylinder was in good agreement with that computed using the PNS code and the FPREM. The measured heat flux to the fin's leading edges agree with that computed with the PNS code and an analysis based on the flow over an infinitely swept cylinder and accounting for the local flow direction.

These observations infer the need to further improve the flow modeling especially in the viscous and separated flow regions. Also the use of a finer mesh may be required to accurately resolve the body geometry and various flow field structures besides the boundary layer.

ACKNOWLEDGMENTS

This research has been sponsored by the Department of the Army, U.S. Army Research Office, Contract No. DAAG29-83-K-0115. The technical liaison is Dr. W. Sturek, Chief, Computational Aerodynamics Branch, U.S. Army Ballistic Research Laboratory, Aberdeen Proving Ground, MD.

The authors gratefully acknowledges Dr. A. B. Wardlaw of the Naval Surface Weapons Center, MD, for providing the SWINT Code. The inputs of Messrs. K.S. Parmar and H. Clisset in this program is also acknowledged.

REFERENCES

Reshotko, E. and Beckwith, I., " Compressible Laminar Boundary Layer Over a Yawed Infinite Cylinder with Heat Transfer and Arbitrary Prandtl Number". NACA Report 1379, 1958.

Rizzi, A., "*Modeling Vortex* Flow Fields by Supercomputers with Super-size Memory," the Aeronautical Journal of the Royal Aeronautical Society, April 1985, Paper No 1291, pp 149-161.

Wardlaw, A.B., Jr., Hackerman, L.B., and Baltakis, F.P., "An Inviscid Computational Method for Supersonic Missile Type Bodies - Program Description and User's Guide," Naval Surface Weapons Center, Dahlgren, Virginia. Paper No. NSWC TR 81-459, December 1, 1981.

Weinacht, P., Guidos, B.J., Sturek, W.B., Hodes, B.A., "PNS Computations for Spinning Shell at Moderate Angles of Attack and for Long L/D Finned Projectiles," AIAA-85-0273, U.S. Army Ballistic Research Laboratory, Aberdeen Proving Ground, MD, AIAA 23rd Aerospace Sciences Meeting, January 14-17, 1985, Reno, Nevada.

LIST OF SCIENTIFIC PERSONNEL

1. Dr. Victor Zakkay
   Professor of Applied Science
   Department of Applied Science
   Director of Antonio Ferri Laboratories

2. Dr. Anthony M. Agnone
   Associate Professor of Applied Science
   Department of Applied Science

3. Mr. Parmar, Kulwarn S.
   Research Assistant

4. Mr. Clisset, Harold
   Research Scientist
   A. Ferri Laboratories

LIST OF PAPERS PUBLISHED ON CONTRACT

1. Agnone, A., Zakkay, V. and Weinacht, P., " Hypersonic Flow Over a Six Finned Configuration" to appear in Experiments in Fluids, Springer Verlag, FRG.

2. Agnone, A., Zakkay, V. and Weinacht, P., "Hypersonic Flow Over a Six Finned Configuration" Presented at the AIAA 23rd Aerospace Sciences Meeting, Reno, NV. January 14-17, 1985. AIAA paper No. 85-0453.

3. Agnone, A., Zakkay, V. and Weinacht, P., "Comparisons of PNS Calculations with Experimental Data of the Hypersonic Flow Over a Six Finned Configuration". Presented at the 66th Semi-annual meeting of the Supersonic Tunnel Association, Albuquerque, N. M. Oct. 6-7, 1986. NYU-DAS-87-158.

4. Agnone, A., Zakkay, V. and Parmar, K. S., "An Economical Data Acquisition System for the NYU A. Ferri Laboratories Hypersonic Wind Tunnel Facility". Presented at the 63rd Semi-annual meeting of the Supersonic Tunnel Association, Dallas, Texas, April 15-16, 1985.

5. Agnone, A., Zakkay, V., "Surface Oil Flow Patterns on a Six Finned Configuration at M= 6.3". Prepared for the 62nd Semi-annual meeting of the Supersonic Tunnel Association, DFVLR Research Center Gottingen, West Germany, October 10-12, 1984.

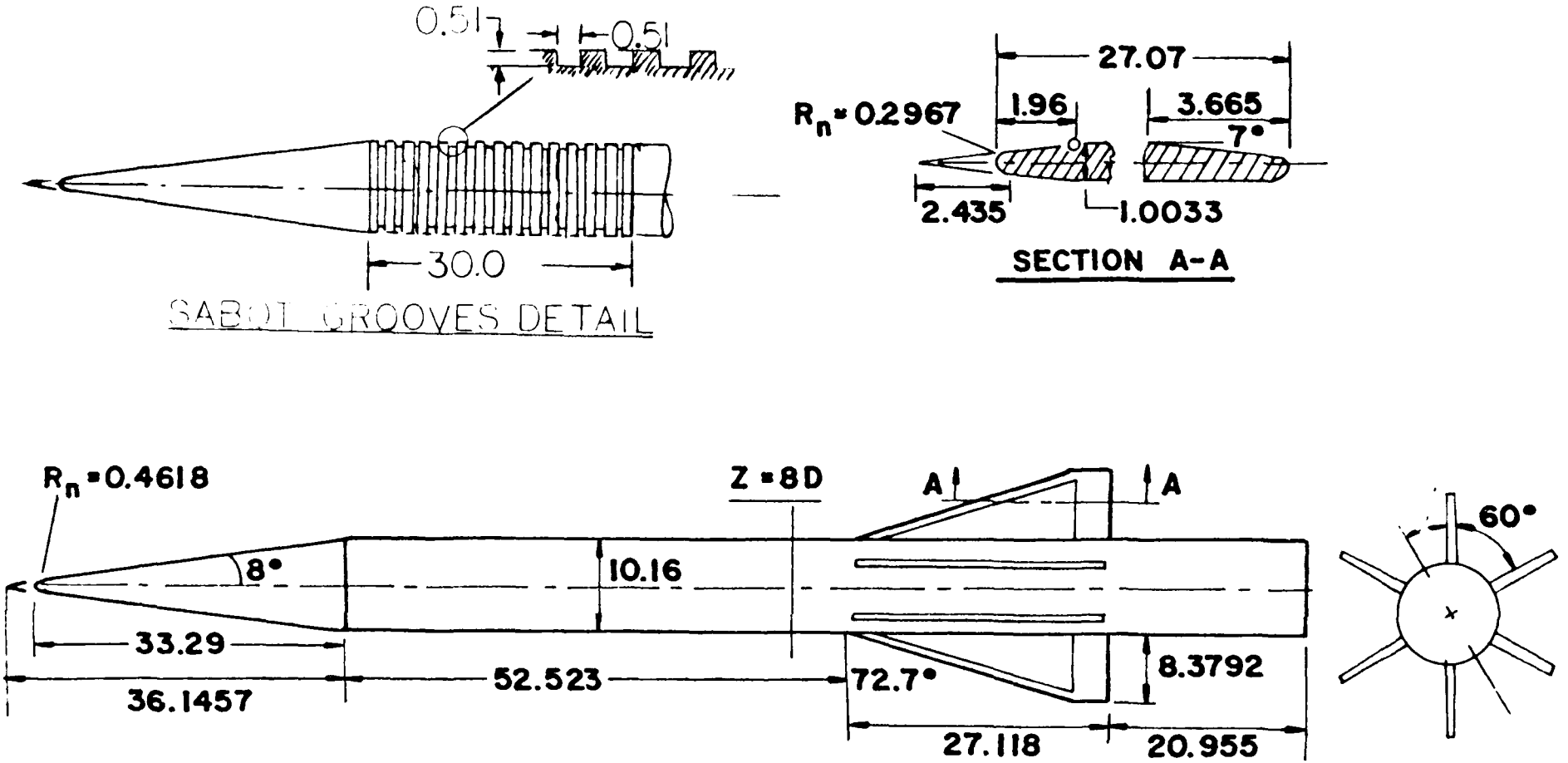

FIG. 1 Windtunnel Model Geometry

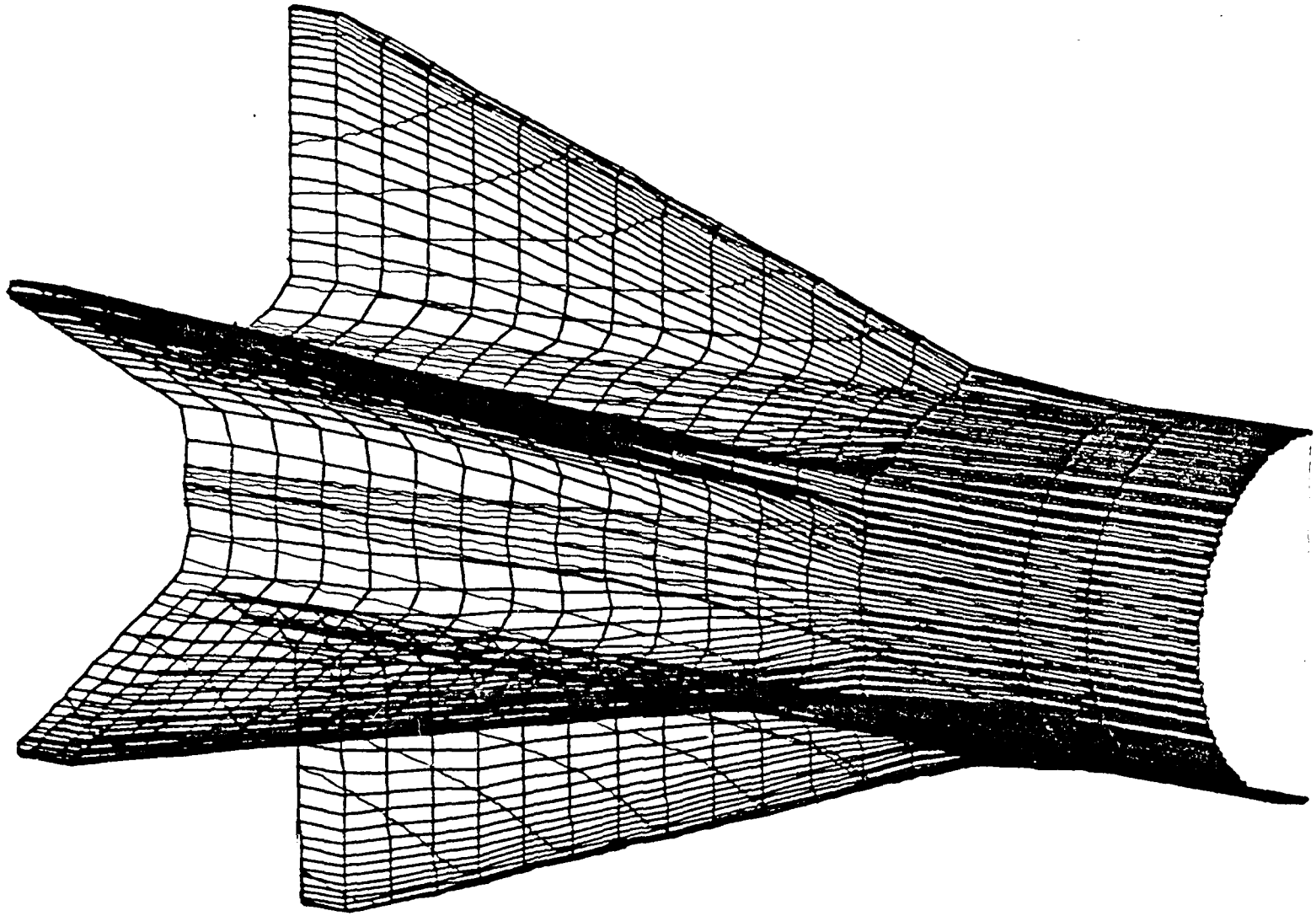

FIG. 2 Surface Streamline Patterns Computed with PNS Code for $\alpha = 0^{o}$

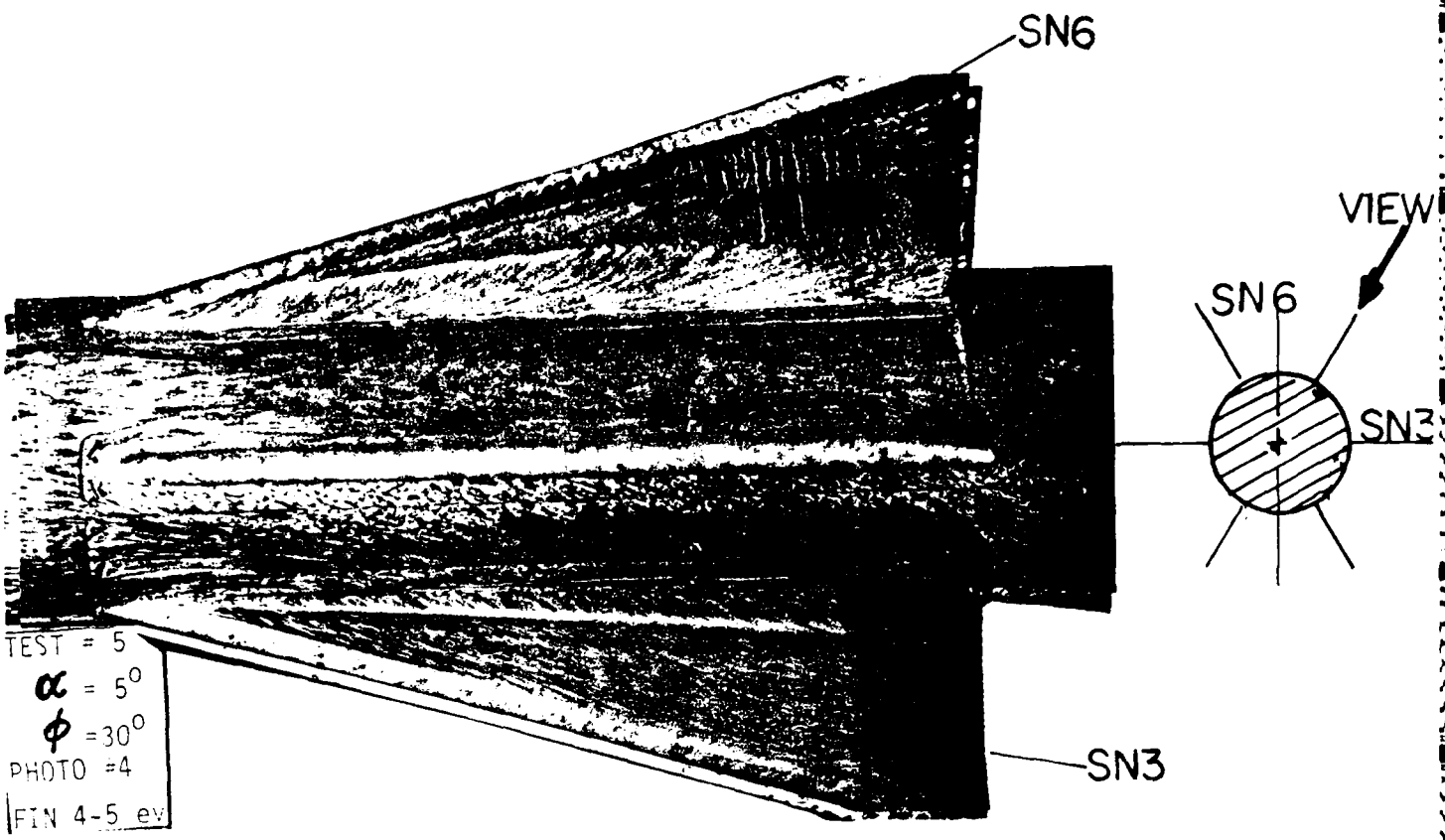

FIG. 3b Typical Oil Flow Patterns on Fins for $\alpha = 5^{o}$ and $\phi = 30^{o}$

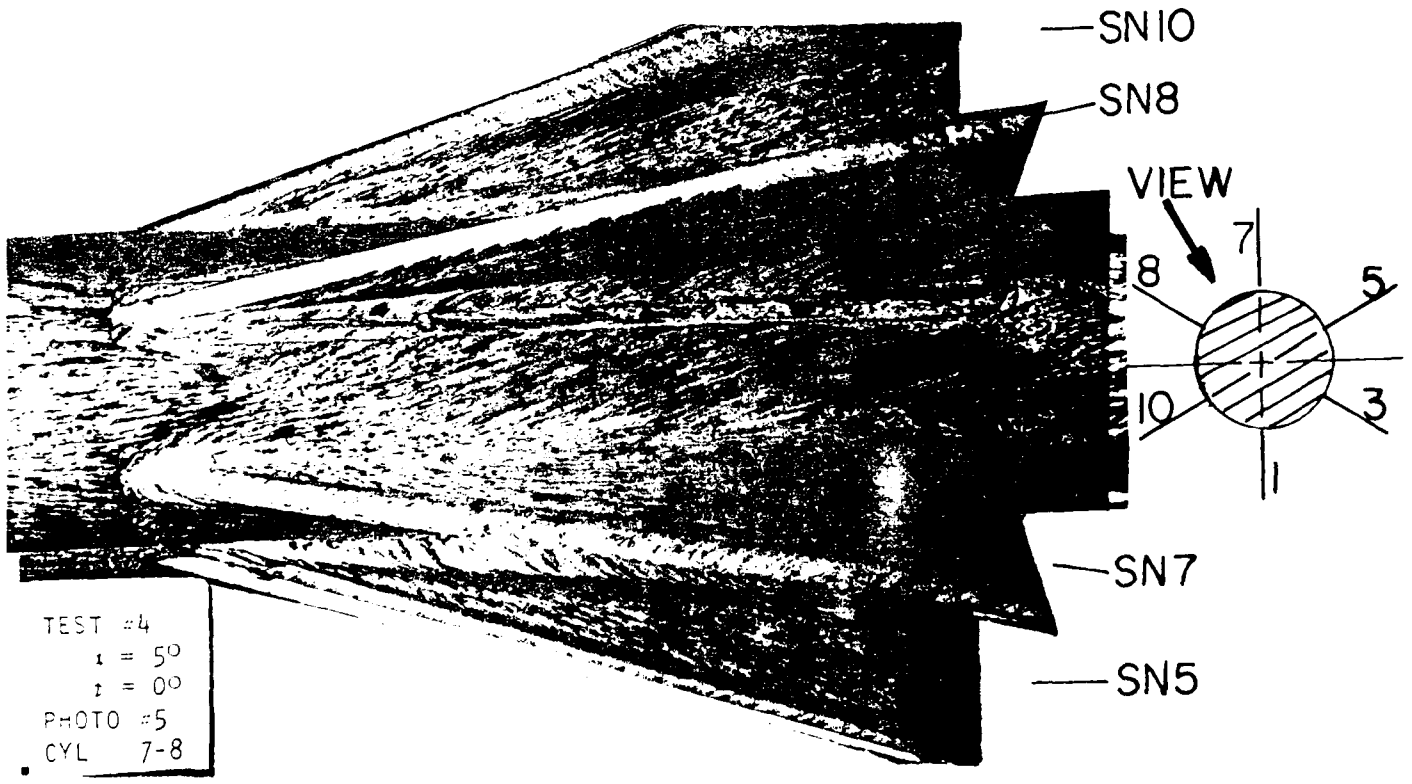

FIG. 3a Typical Oil Flow Patterns on Fins for $\alpha = 5^{o}$ and $\phi = 0^{o}$

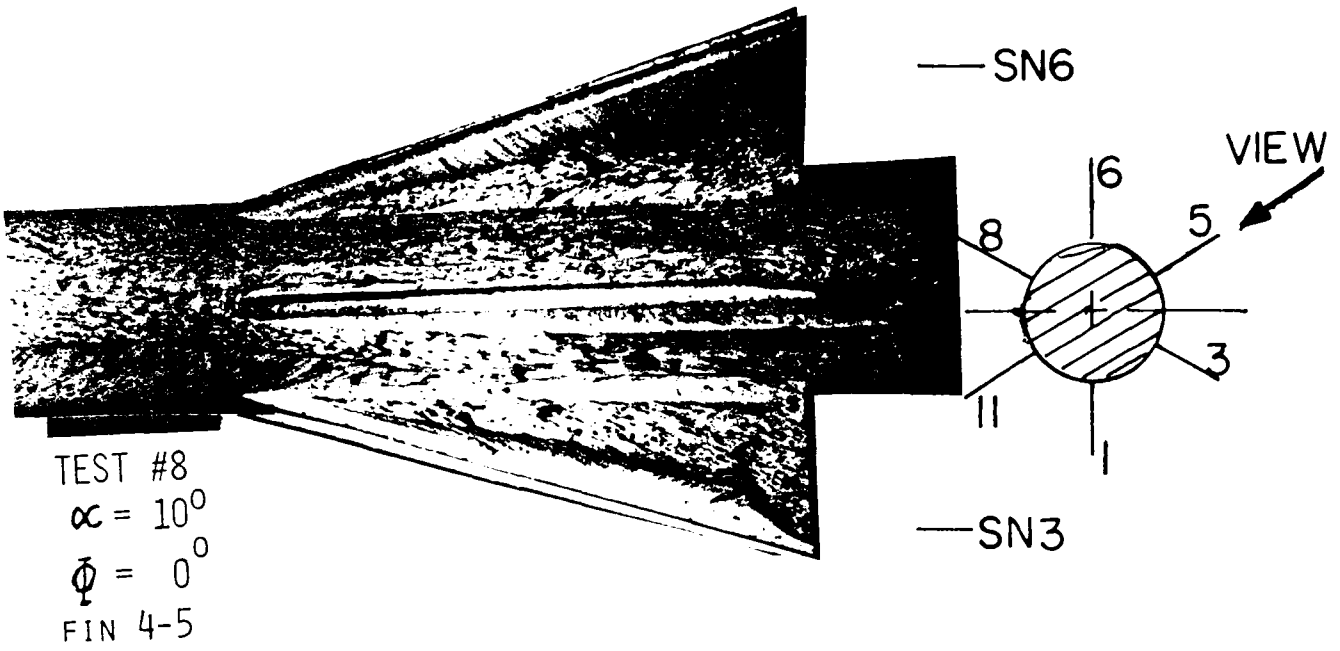

4a. Typical Oil Flow Patterns on Fins for $\alpha = 10°$ and $\Phi = 0°$

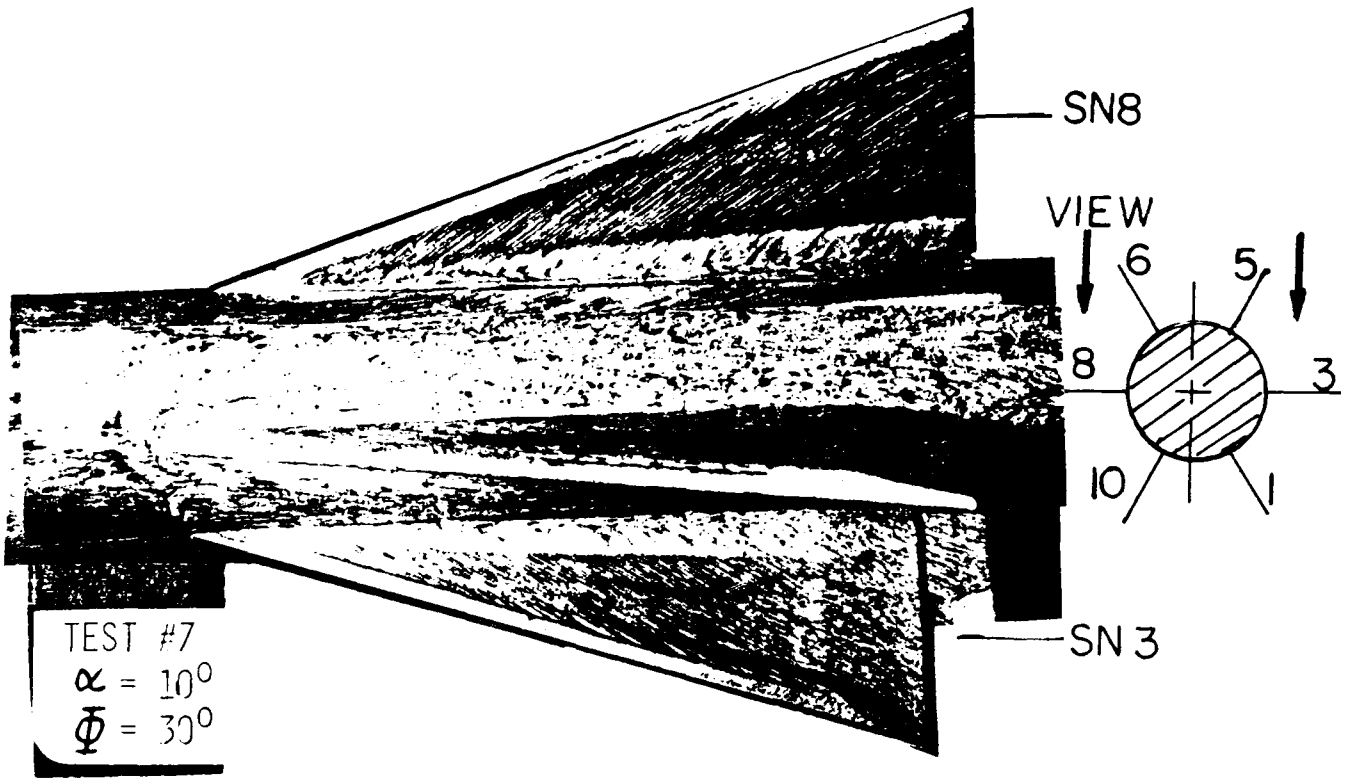

4b. Typical Oil Flow Patterns on Fins for $\alpha = 10°$ and $\Phi = 30°$

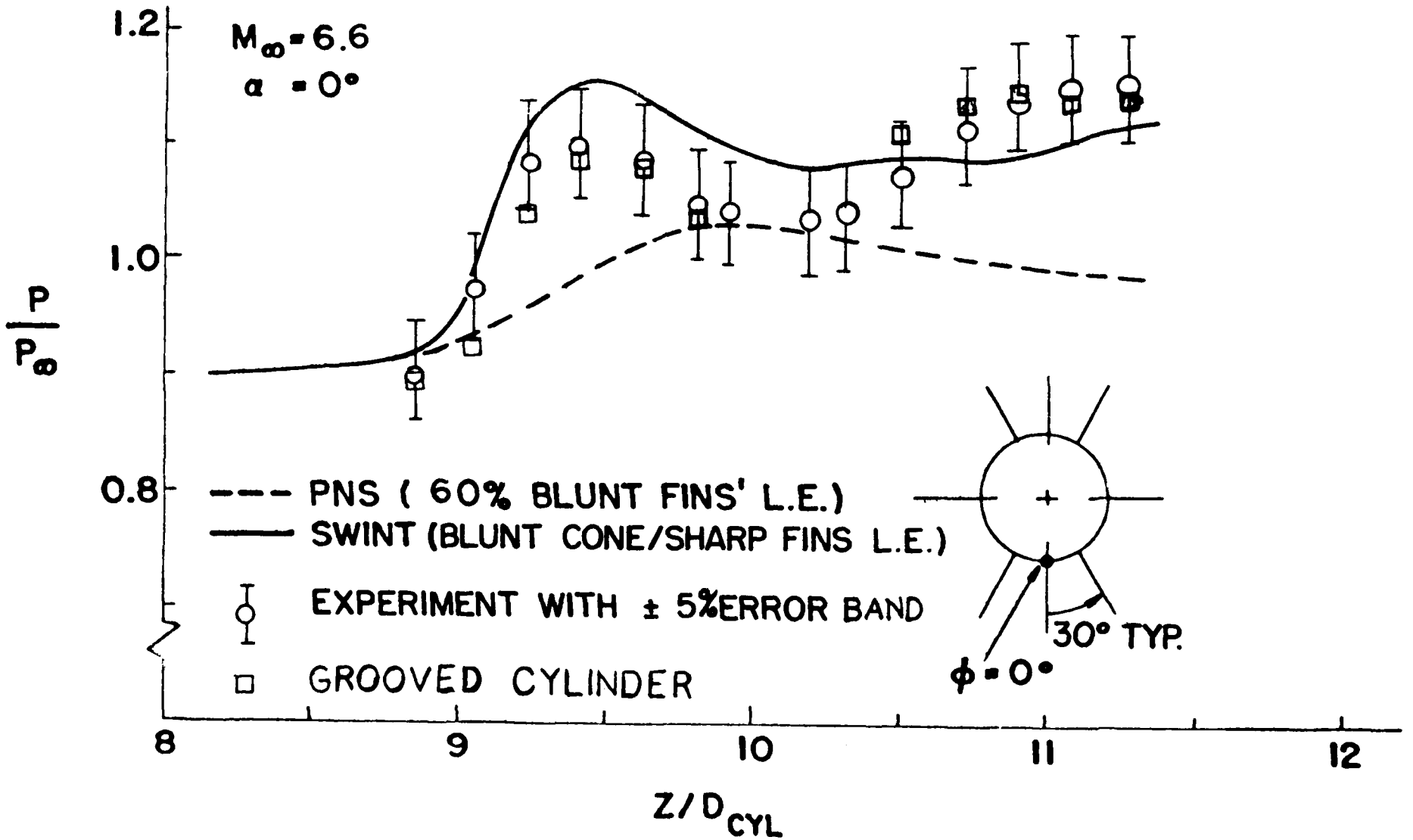

FIG. 5 Pressure Distribution on the Cylinder Midway Adjacent Fins for $\alpha=0^o$

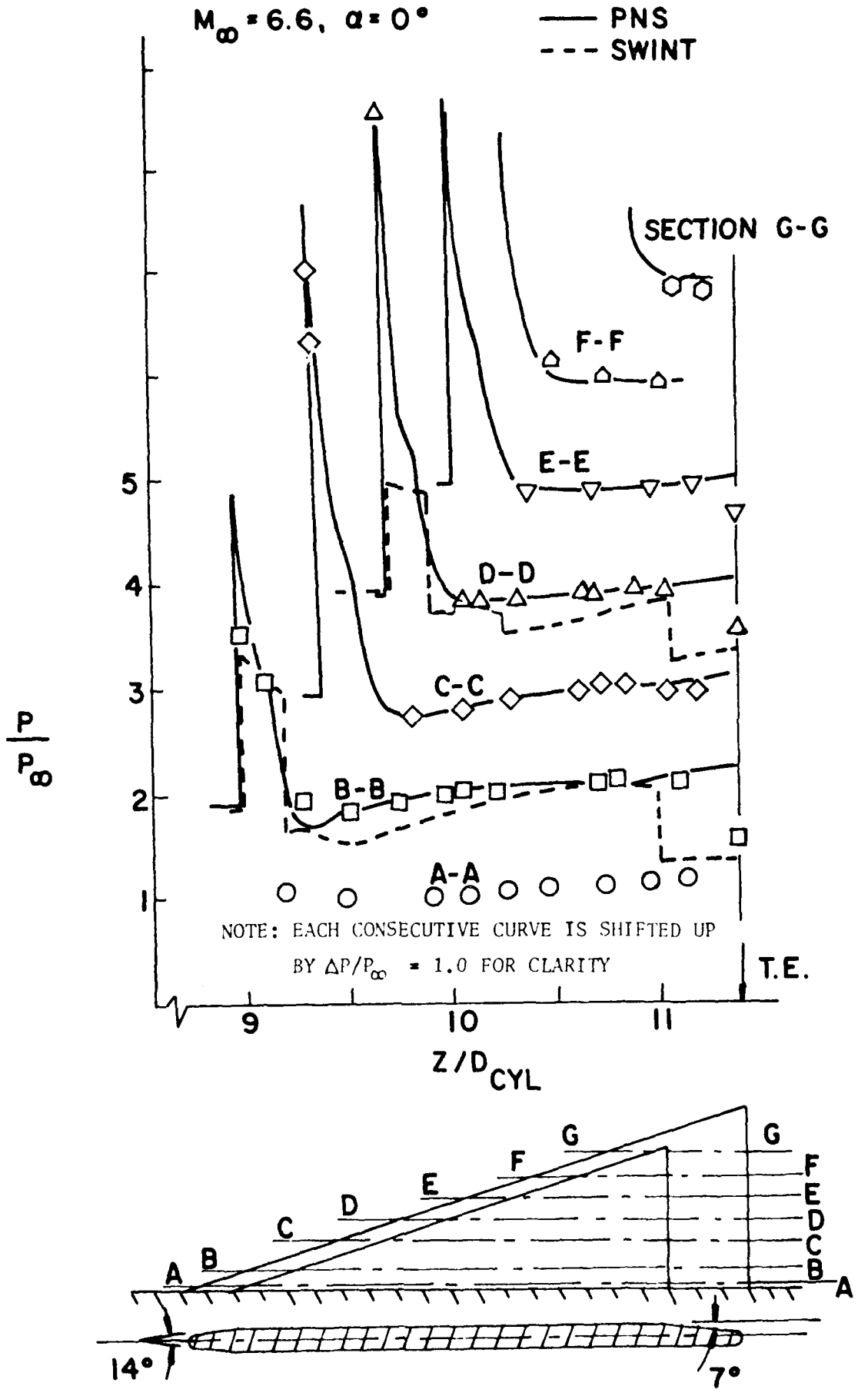

FIG. 6 Pressure Distributions at Several Outboard Stations of a Typical Fin α=0

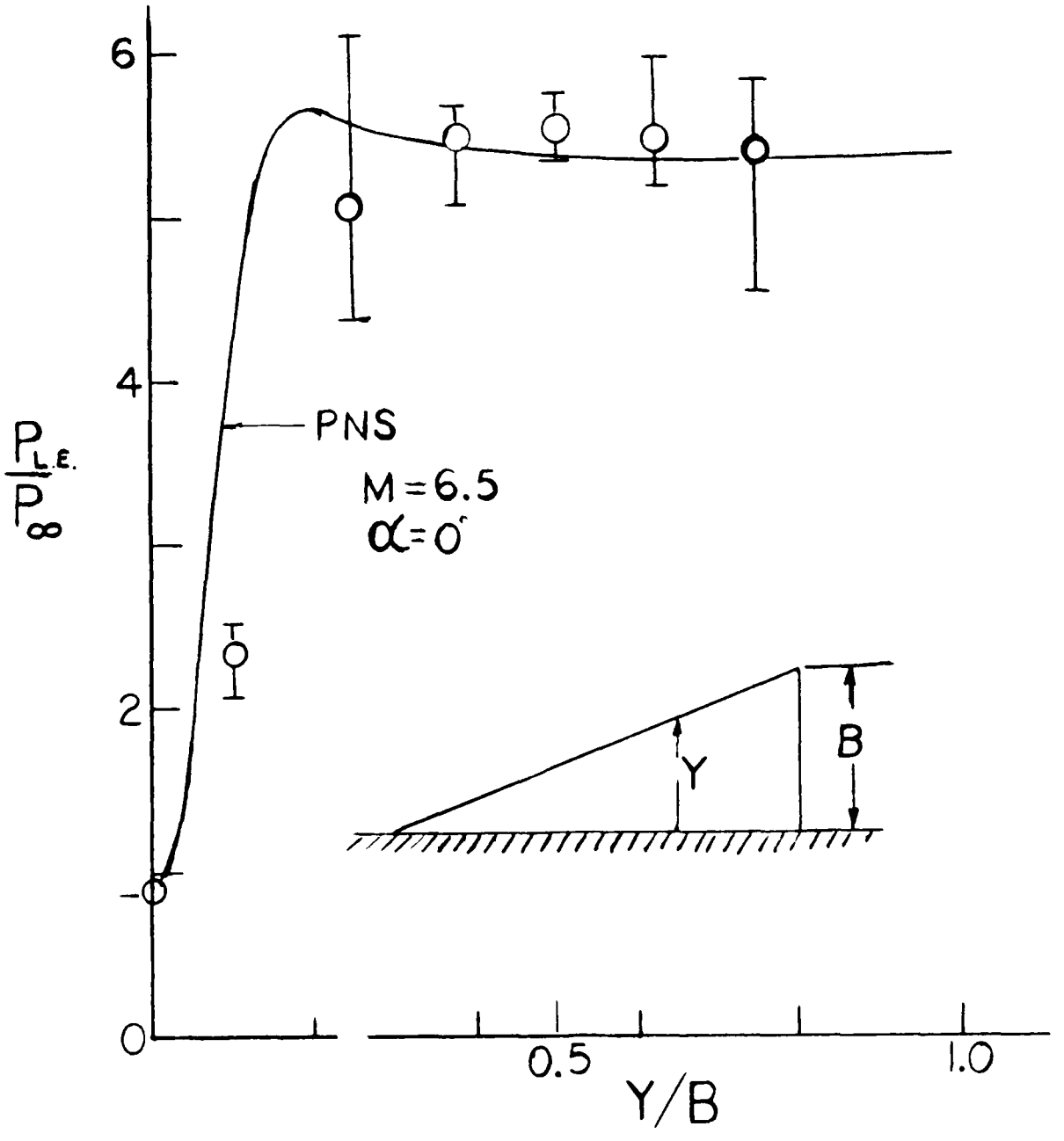

FIG. 7 Pressure Distribution Along a fin Leading Edge (Stagnation Line)

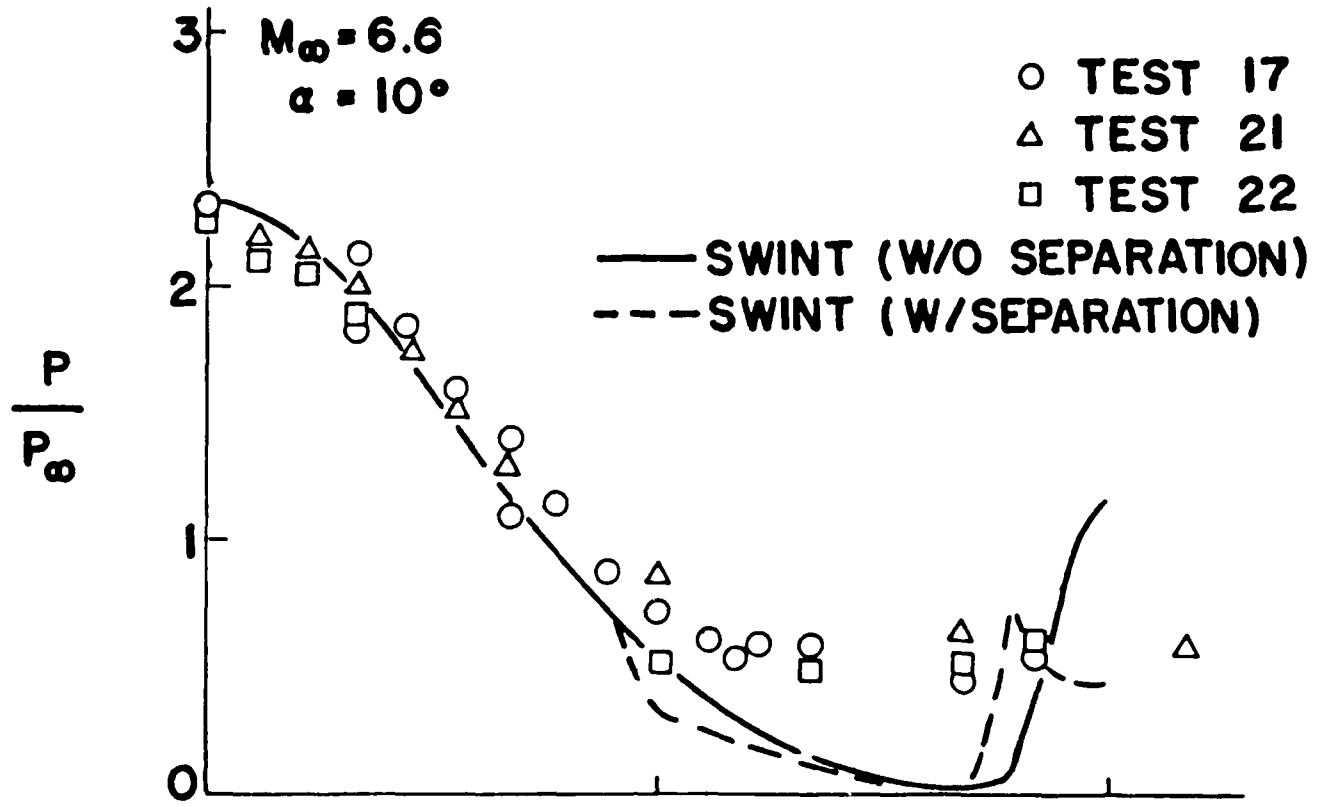

FIG. 8b Pressure Distribution around the Cylinder Upstream of the Fins for $\alpha=10^o$

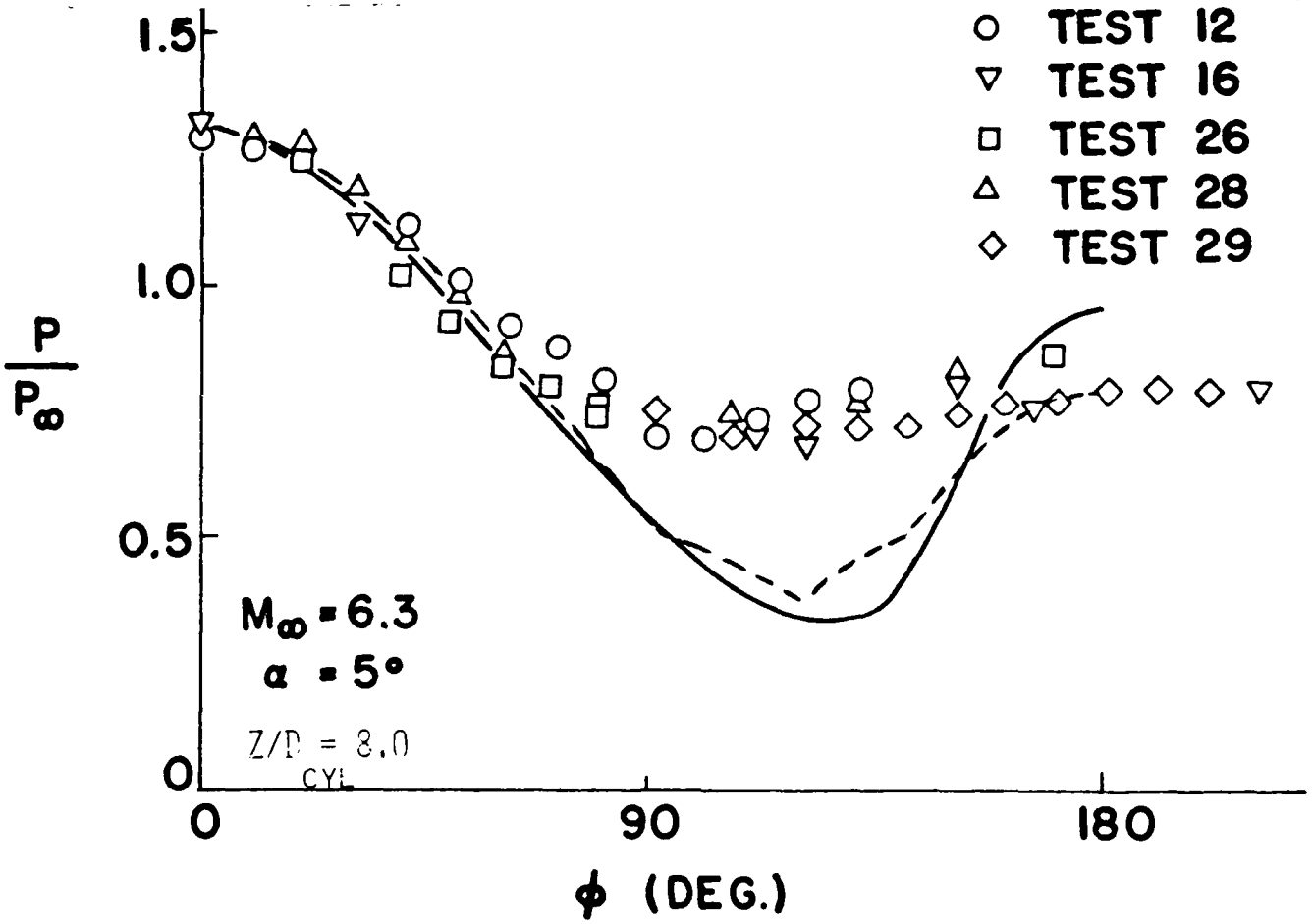

FIG. 8a Pressure Distribution around the Cylinder Upstream of the Fins for $\alpha=5^o$

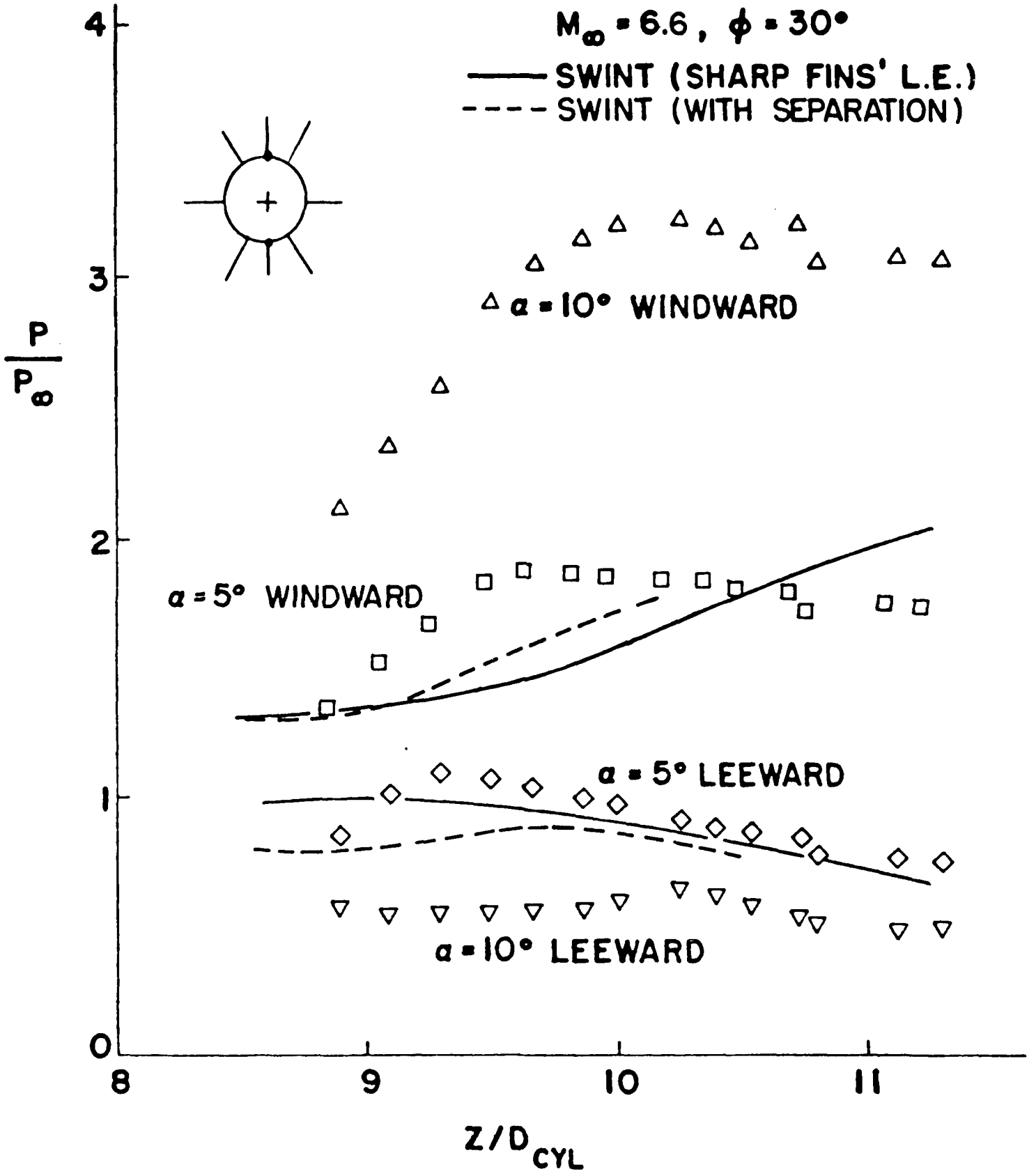

FIG. 9 Pressure Distribution on the Most Windward and Leeward Rays of the Cylinder Midway Adjacent Fins For $\phi = 30^0$ and for $\alpha = 5^0$ and $\alpha = 10^0$

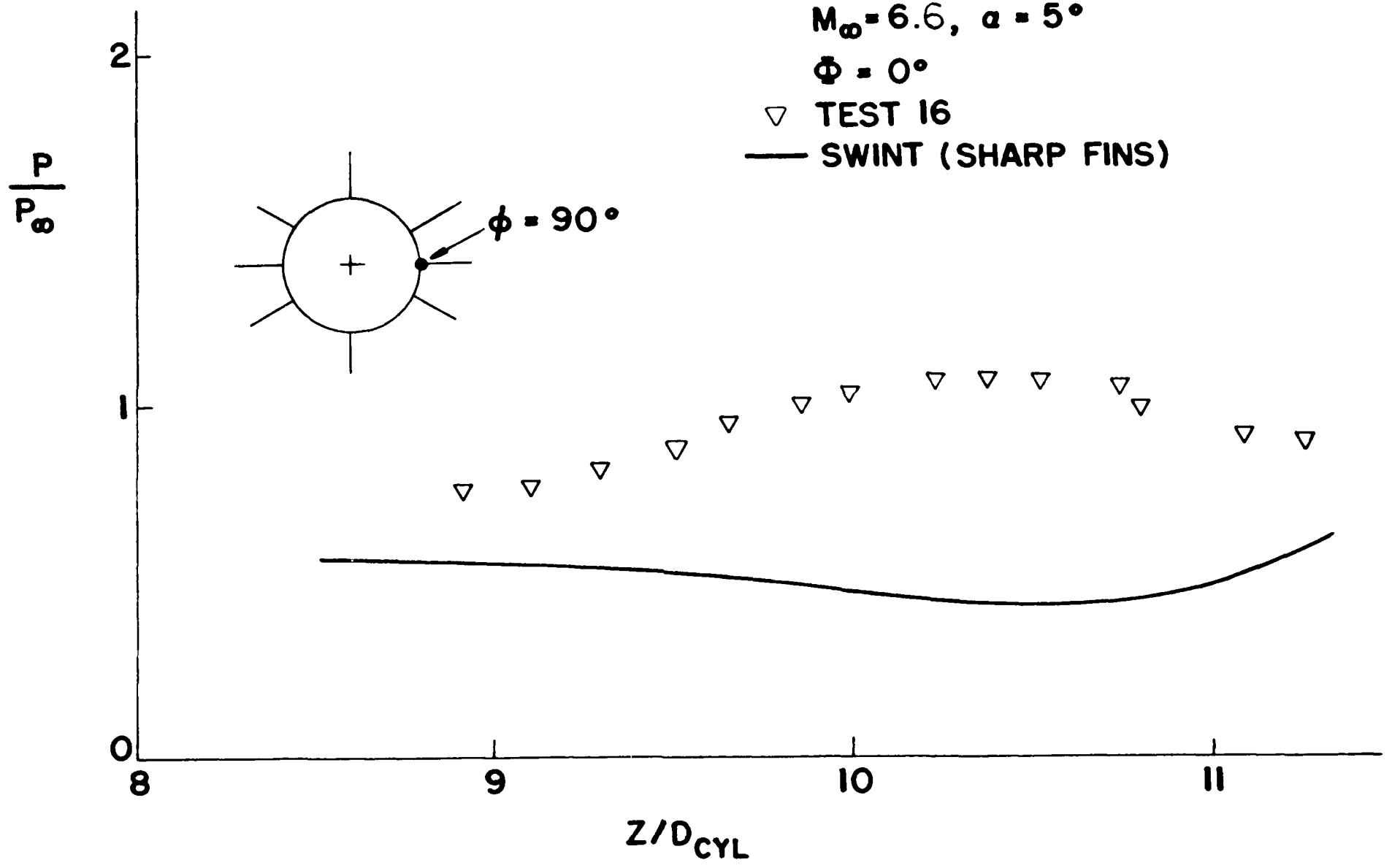

FIG. 10 Pressure Distribution on the Side Ray of the Cylinder for $\alpha=5^0$

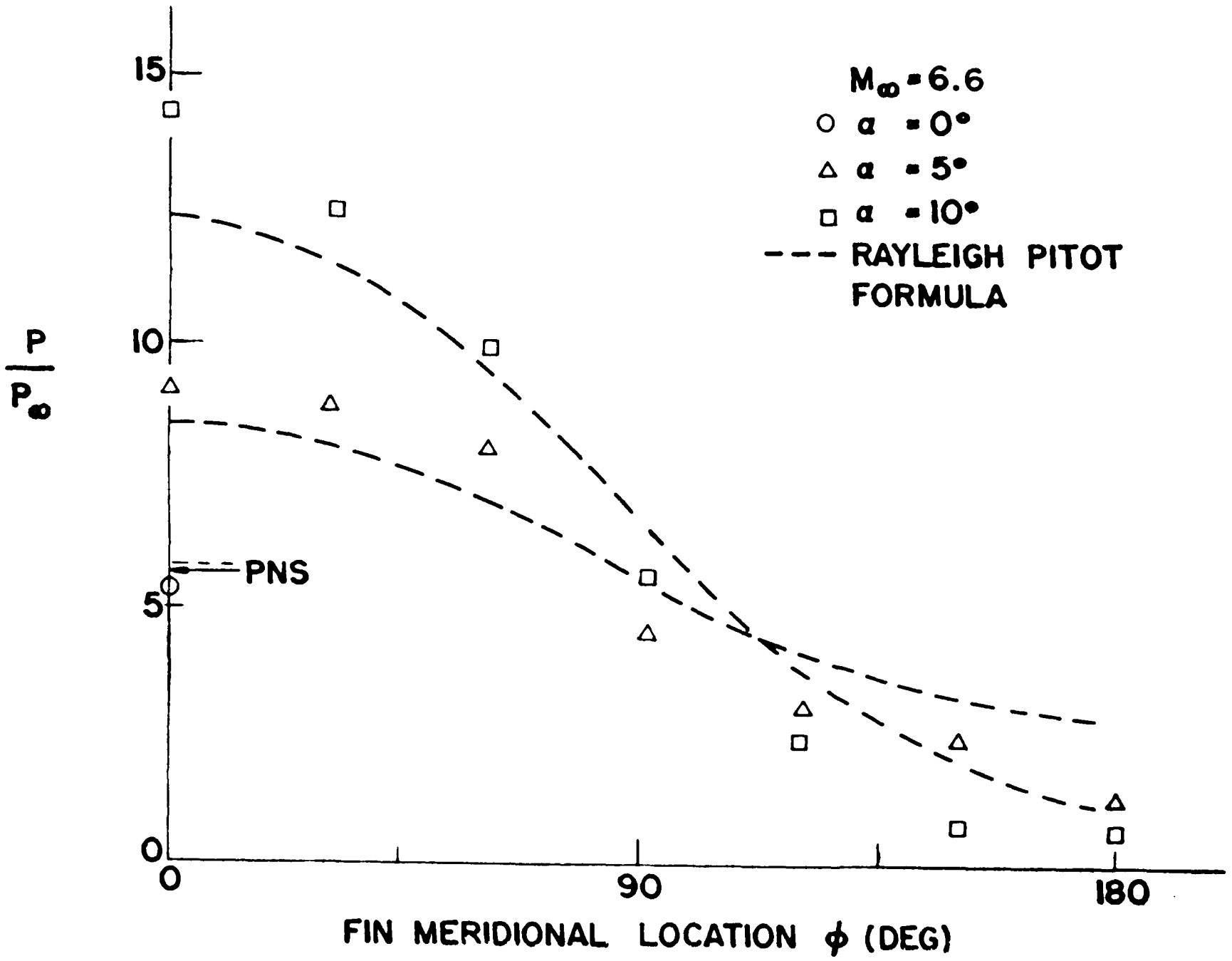

FIG. 11 Pressure at Midspan of Fins Leading Edge for $\alpha = 5^0$ and $\alpha = 10^0$

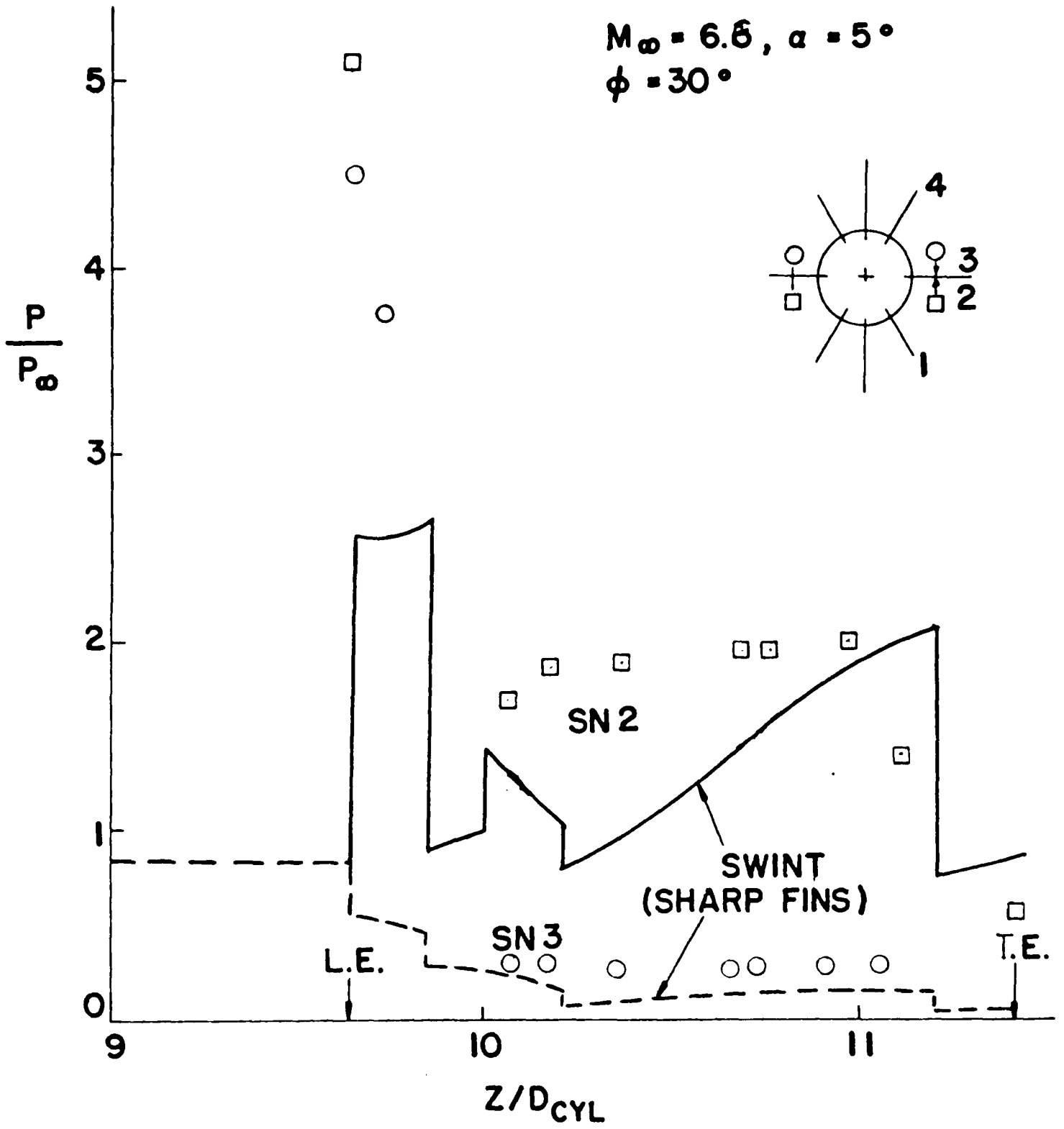

FIG. 12 Pressure Distributions Along a Section at Midspan of the Horizontal Fins' Windward and Leeward Surfaces for $\phi = 30^{o}$, and $\alpha = 5^{o}$

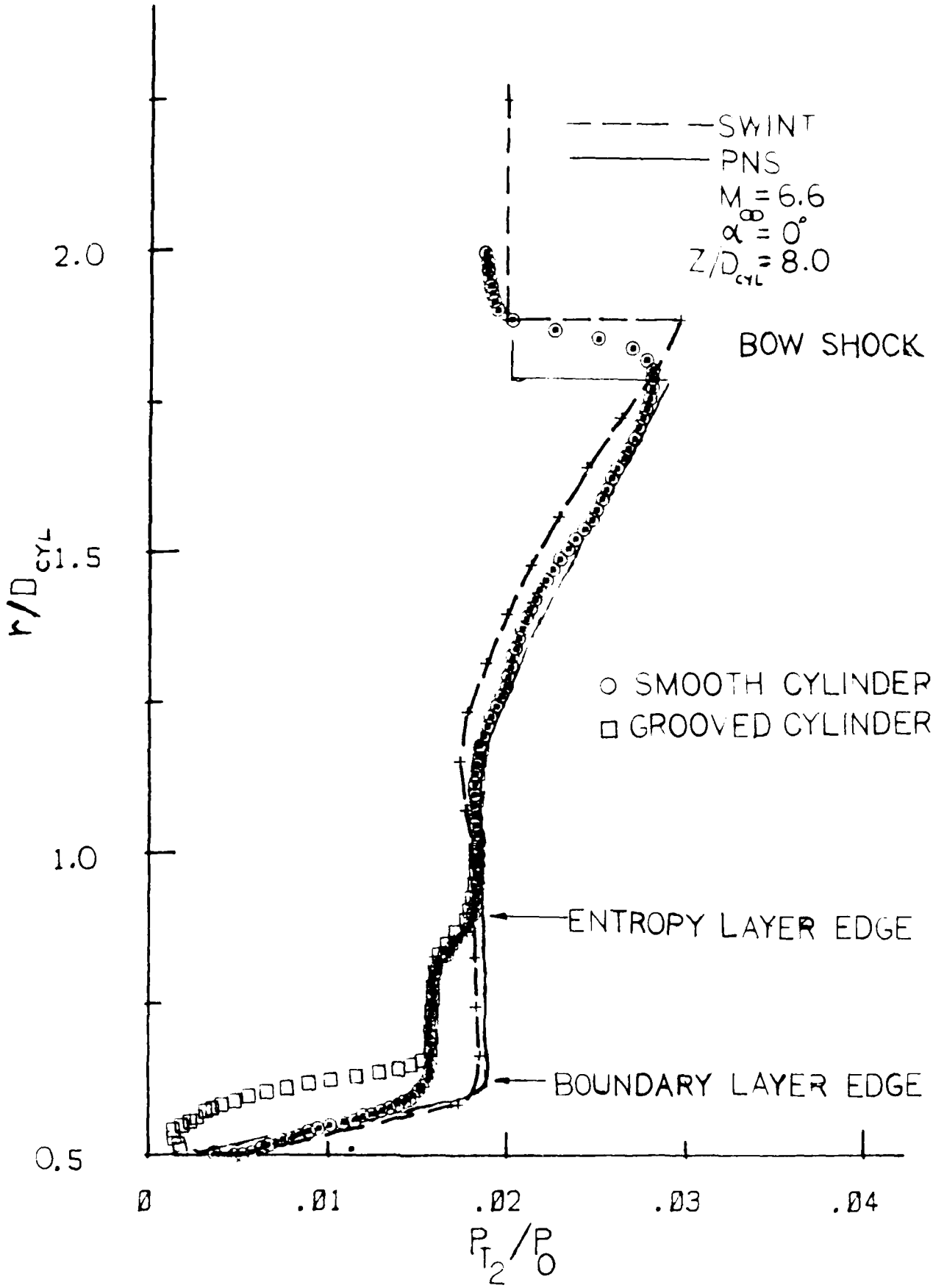

FIG. 13a Pitot Pressure Profiles Upstream of the Fins for the Smooth and Grooved Cylinder for $\alpha = 0^0$

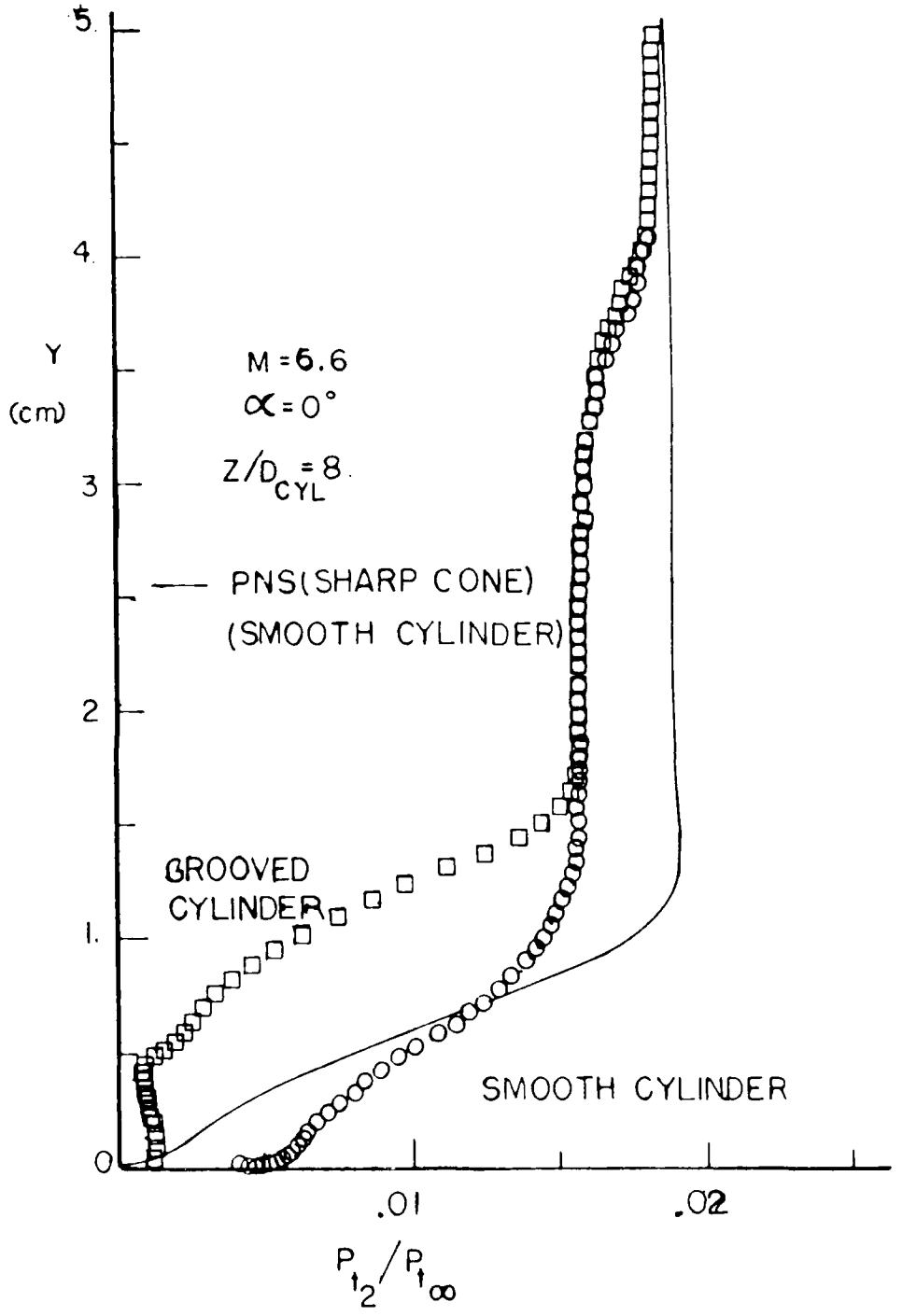

FIG.13b Pitot Pressure Profile in the Boundary Layer Upstream of the Fins for the Smooth and Grooved Cylinders and for $\alpha = 0^{o}$

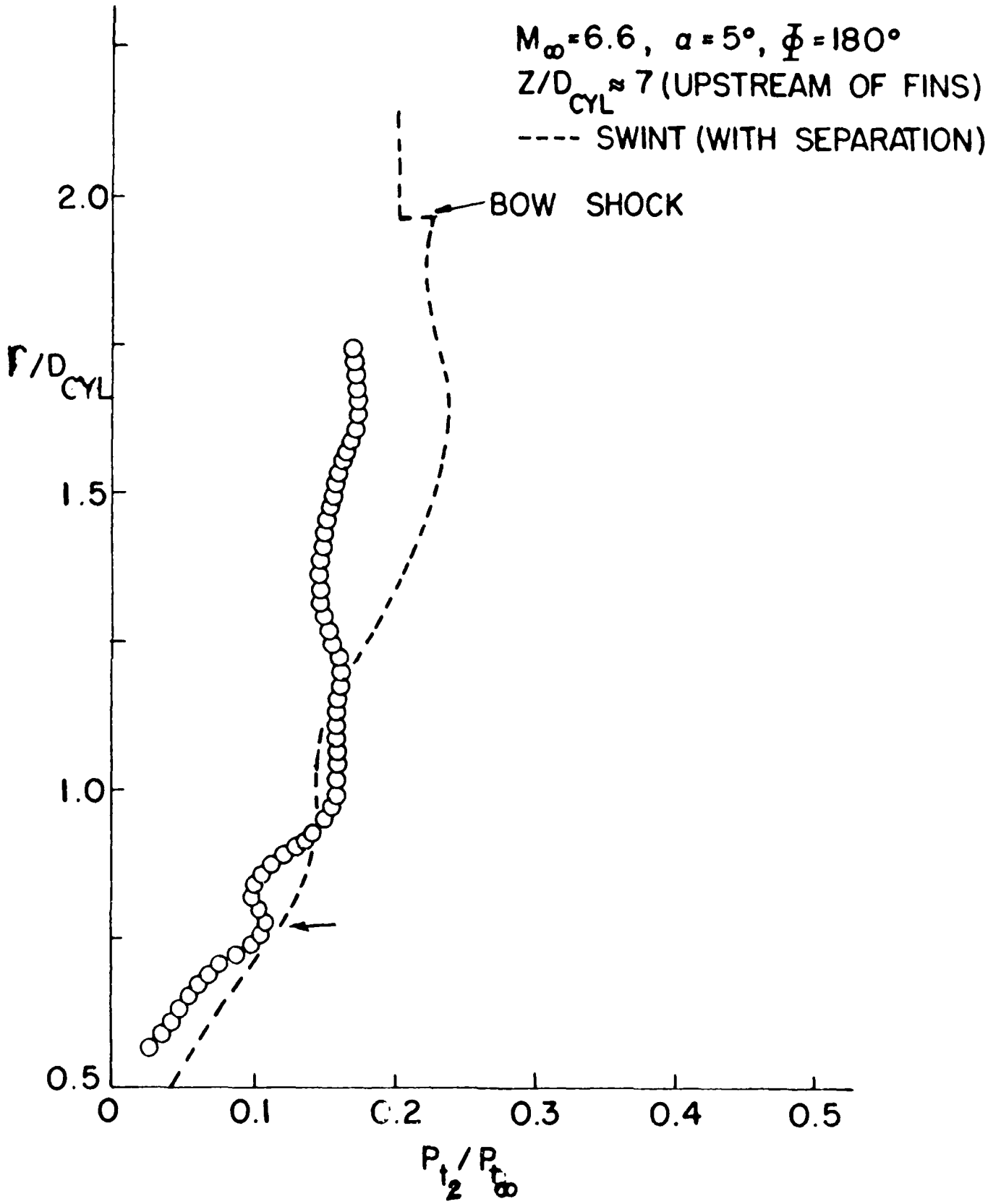

FIG. 14 Pitot Pressure Profile Upstream of Fins on Leeward Side of the Pitch Plane for $\alpha = 5^0$

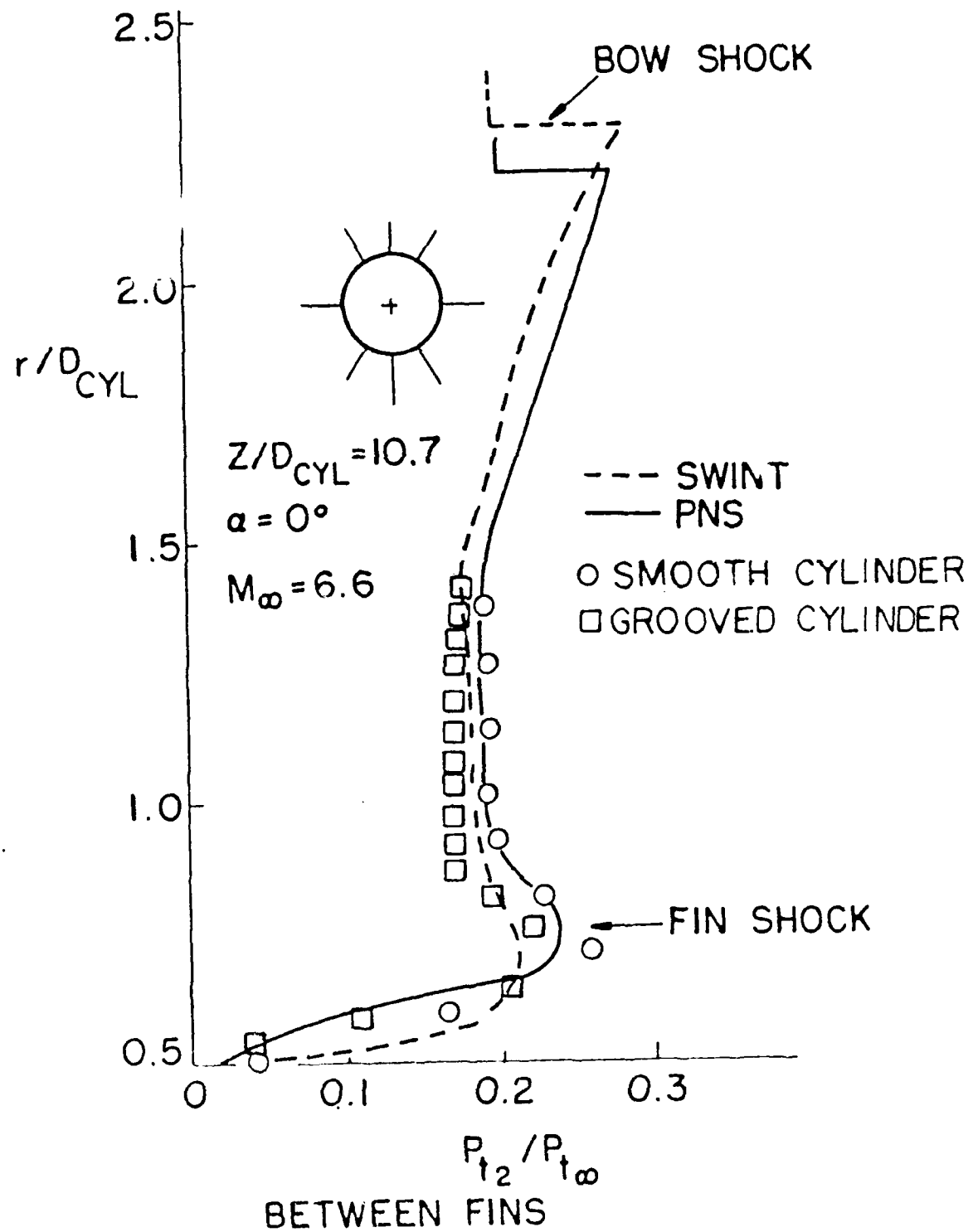

FIG. 15 Pitot Pressure Profile in Fin Region Midway Adjacent Fins for $\alpha = 0^{o}$

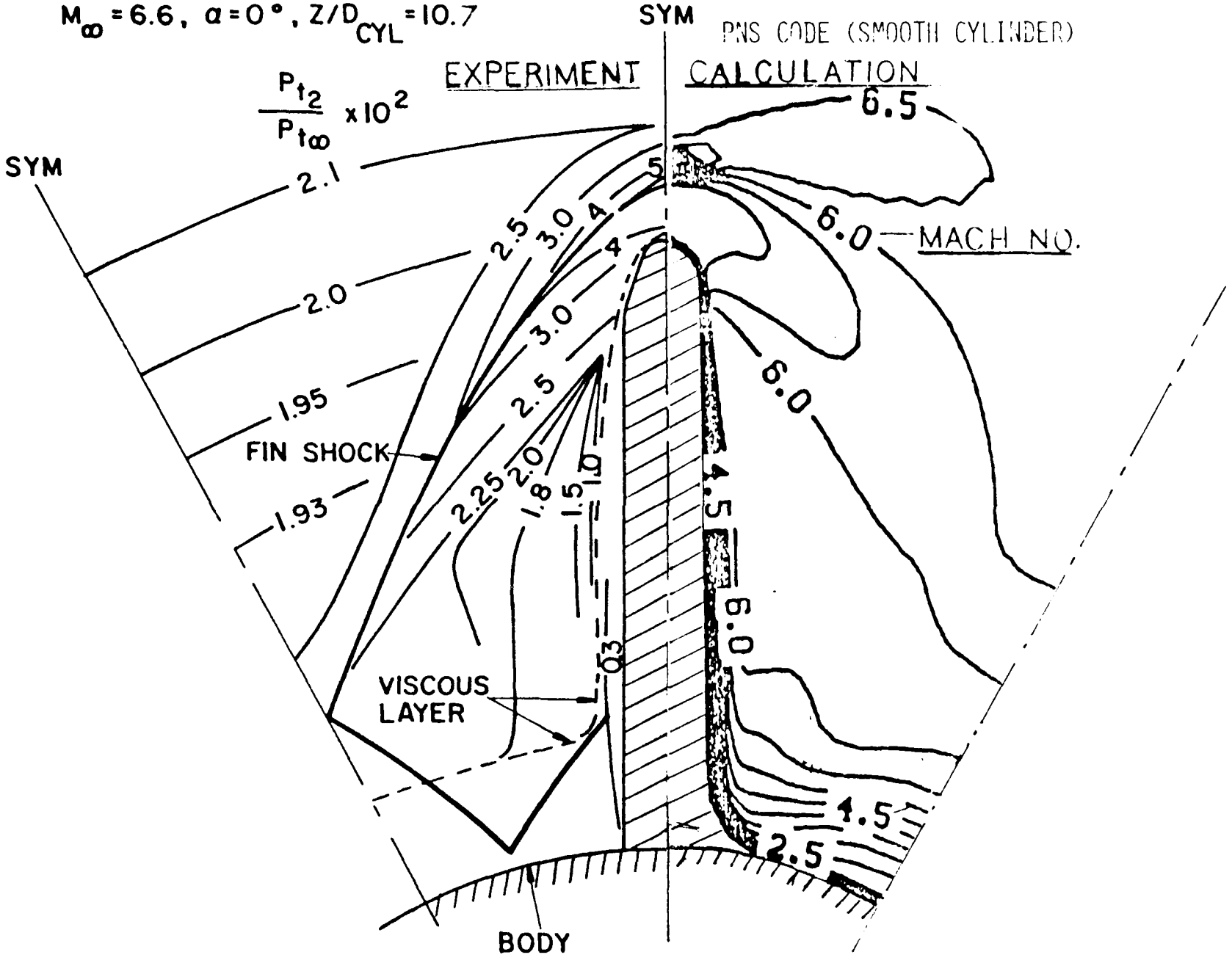

FIG. 16a Pitot Pressure Contours Around a Typical Fin for $\alpha = 0^o$ - Smooth Cylinder

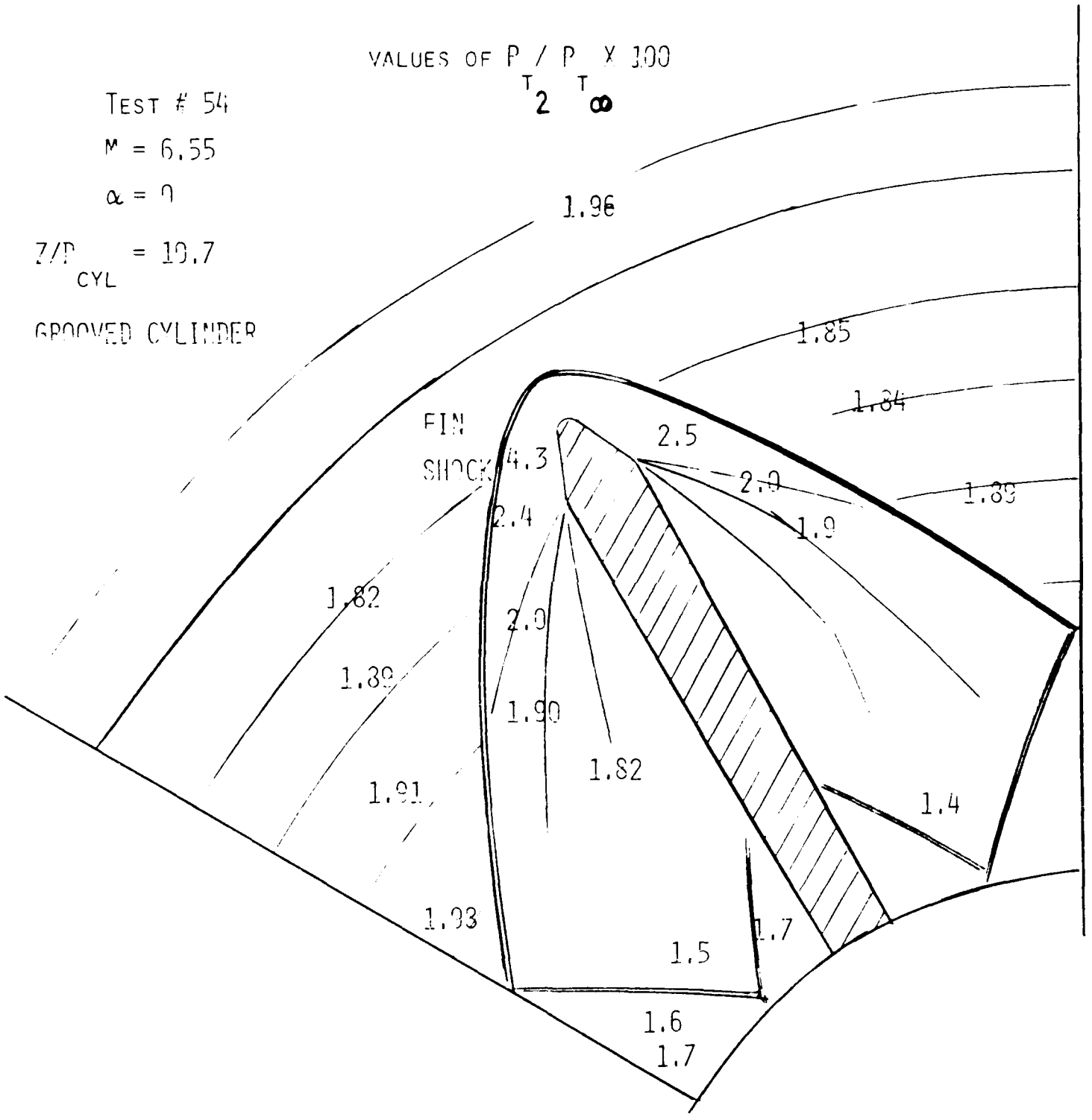

FIG. 16b Pitot Pressure Contours Around a Typical Fin for $\alpha = 0^{o}$- Grooved Cylinder

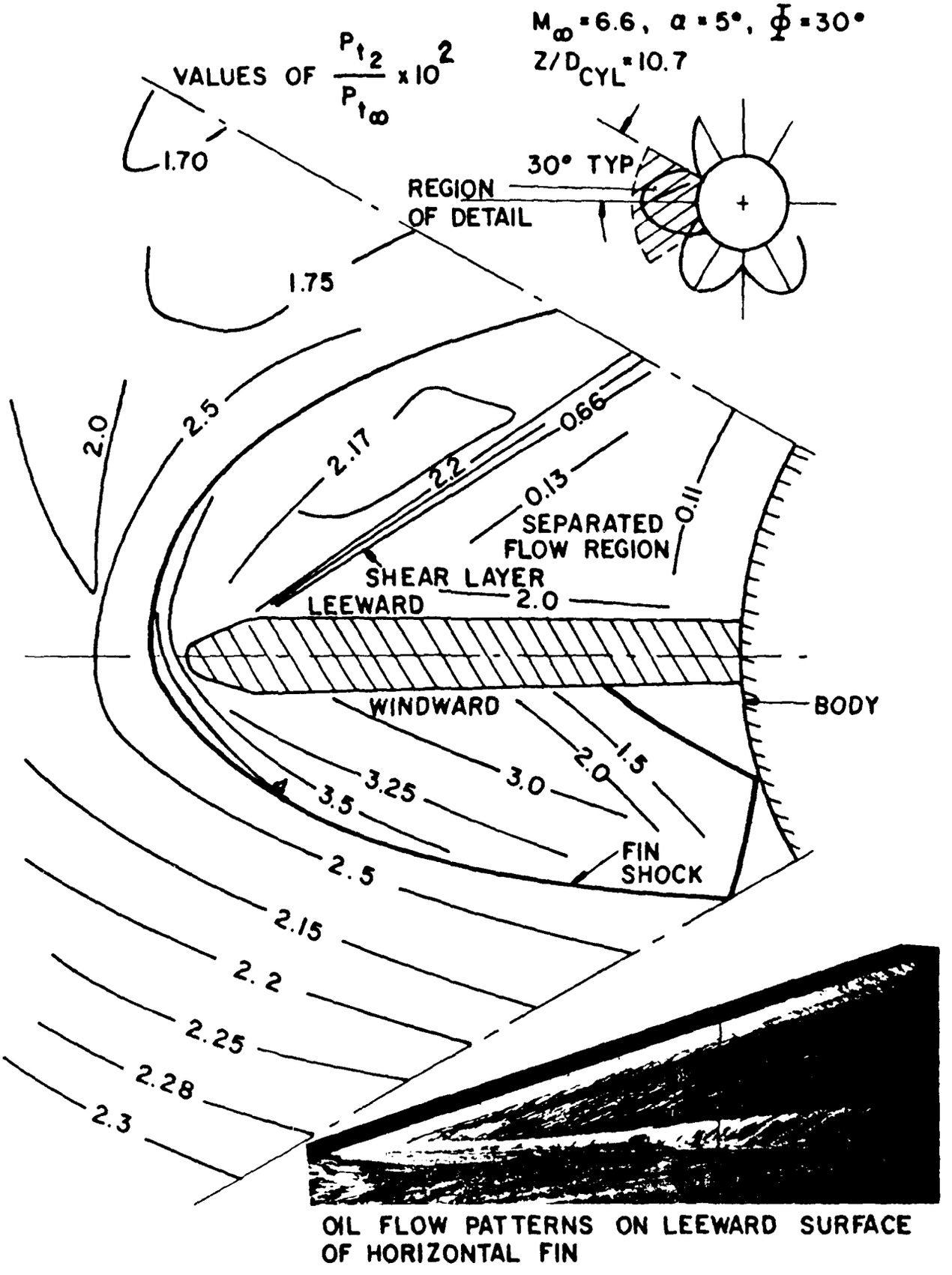

OIL FLOW PATTERNS ON LEEWARD SURFACE OF HORIZONTAL FIN

FIG. 17 Pitot Pressure Contours in a 60^o Sector Around the Horizontal Fin for $\alpha = 5^o$ and $\phi = 30^o$

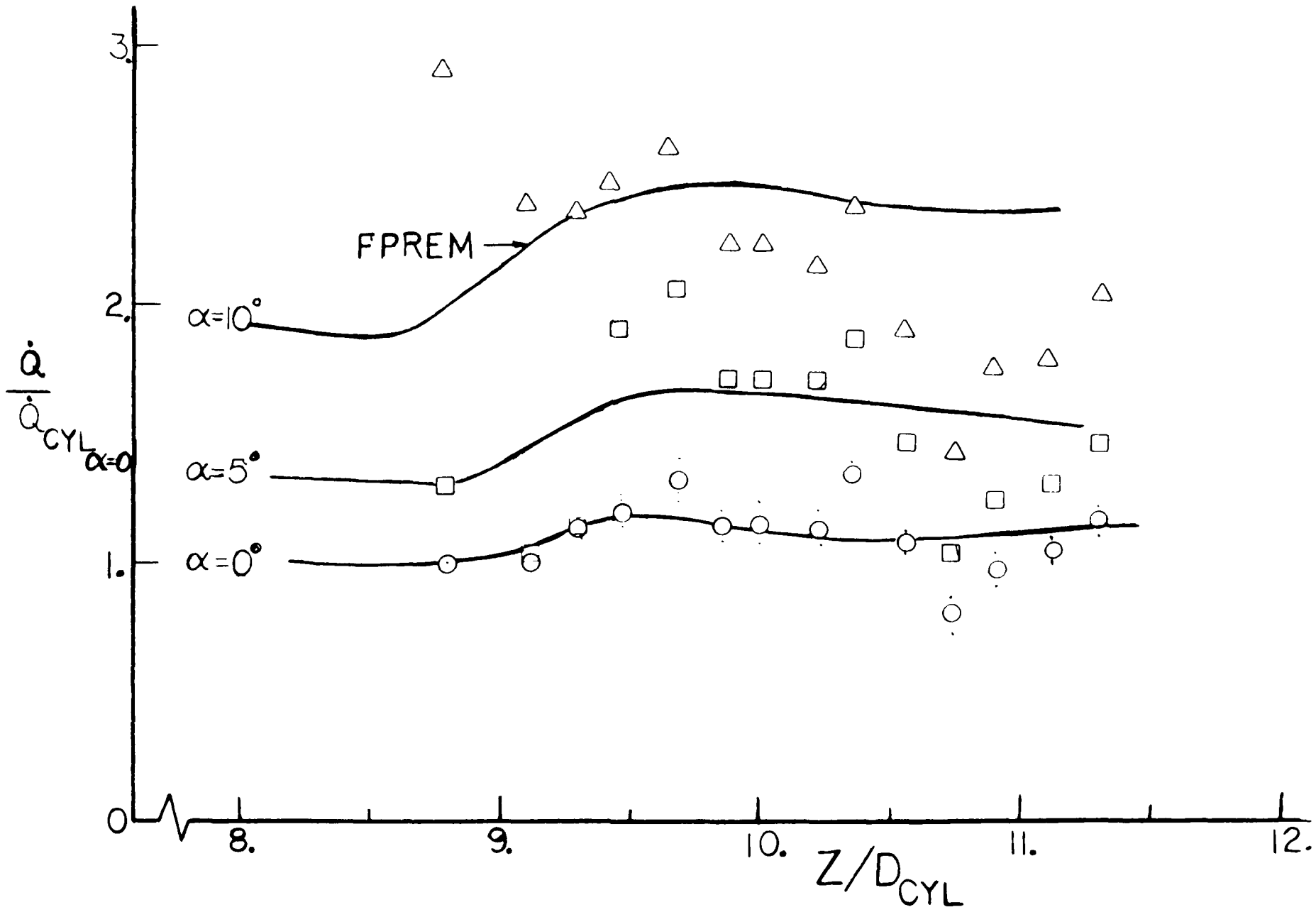

FIG. 18 Heat Flux Along the Most Windward Ray of the Cylinder and Midway Adjacent Fins for $\phi = 30^{o}$

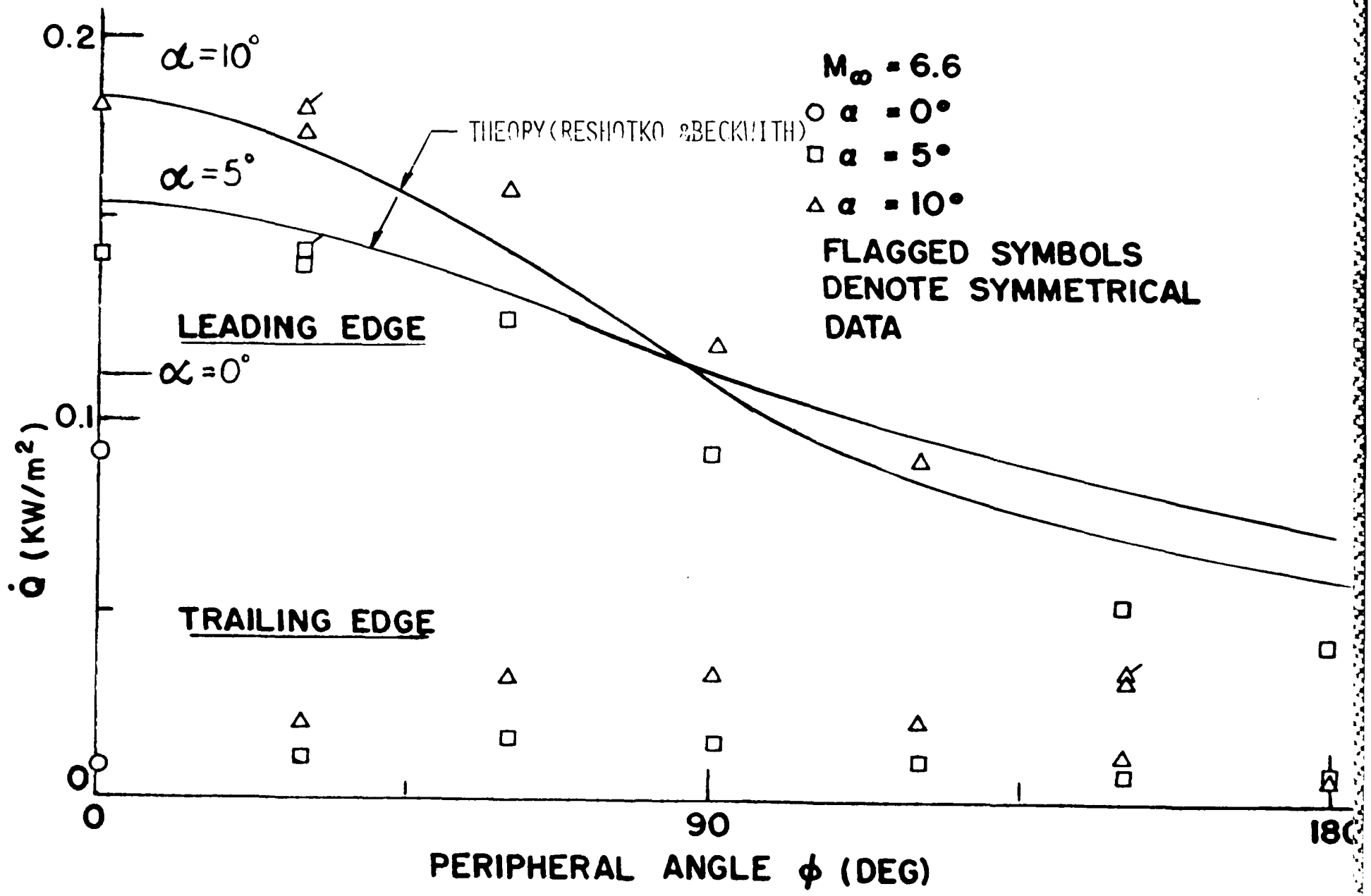

FIG. 19 Heat Flux at Midspan of the Fins' Leading and Trailing Edges for $\alpha = 5^{o}, 10^{o}$

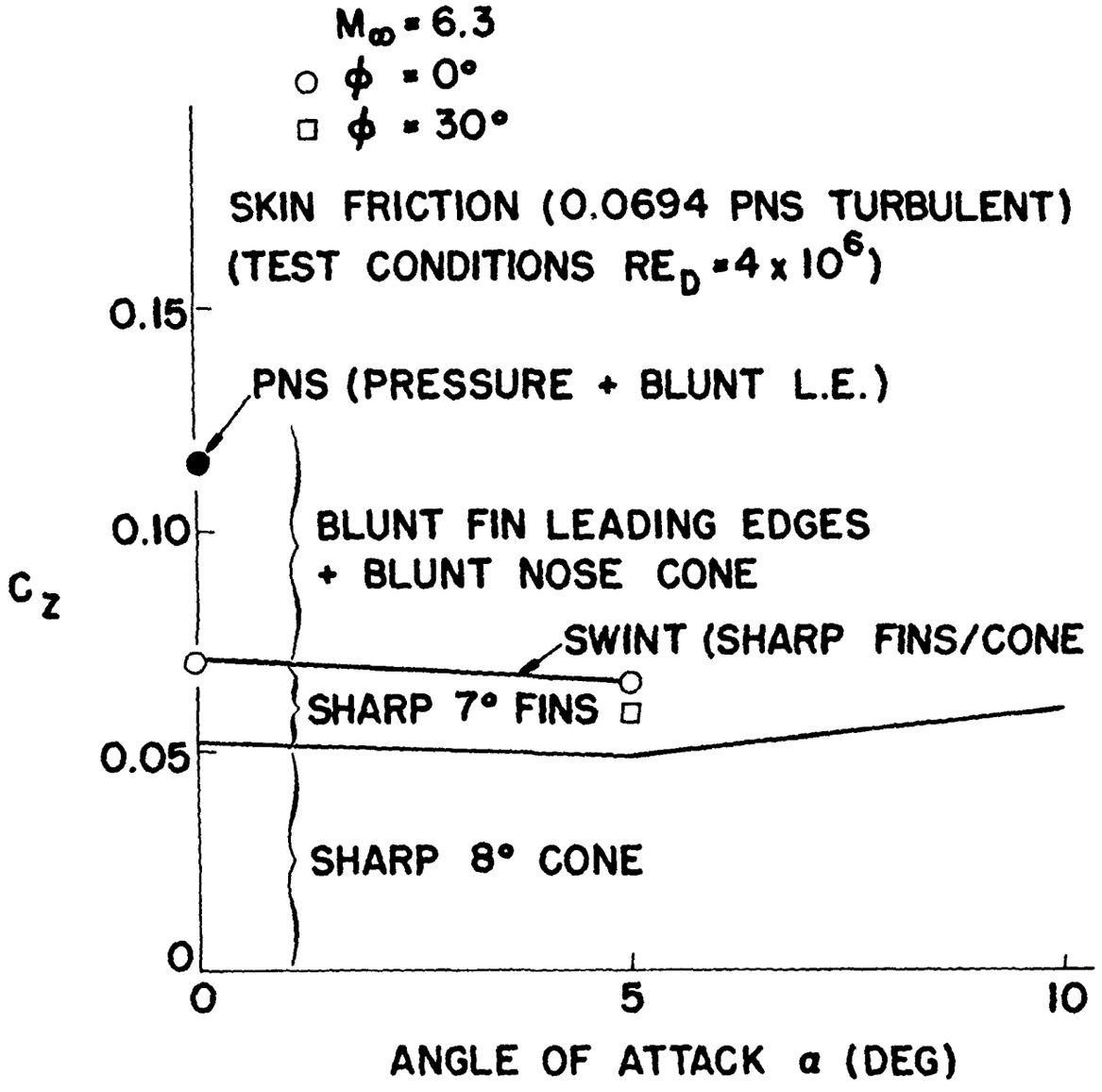

FIG. 20 Axial Force Coefficient of the Complete Configuration

END

DATE

FILMED

5-88

DTIC